Research Square

Preprints are preliminary reports that have not undergone peer review.
They should not be considered conclusive, used to inform clinical practice,
or referenced by the media as validated information.

Geometric Curvature in Out-of-plane Flexural Design of Unreinforced Masonry Walls

John Mary Joseph Yiga

yigajmj@gmail.com

Makerere University

Allan Ray Okodi

Makerere University

Moses Jr Matovu

Makerere University

Research Article

Keywords: Curved Masonry walls, Simplified Micro-Modelling, Out-Of-Plane loads

Posted Date: May 18th, 2026

DOI: https://doi.org/10.21203/rs.3.rs-9301959/v1

License: This work is licensed under a Creative Commons Attribution 4.0 International License.
Read Full License

Additional Declarations: No competing interests reported.

GEOMETRIC CURVATURE IN OUT-OF-PLANE FLEXURAL DESIGN OF UNREINFORCED MASONRY WALLS

John Mary Joseph Yiga[1*], **Allan Ray Okodi**[1], **Moses Jr Matovu**[1],
yigajmj@gmail.com, allan.okodi@mak.ac.ug, mmatovujr@gmail.com,

[*]Corresponding Author: John Mary JosephYiga
[1]Department of Civil and Environmental Engineering, Makerere University
Kampala, Uganda

ABSTRACT

Unreinforced masonry (URM) walls are highly susceptible to out-of-plane (OOP) loading, often failing in brittle flexure. Existing analytical formulations and design provisions are largely tailored for planar walls that do not apply to curved masonry walls, which offer an underexplored opportunity to enhance lateral resistance through architectural form. This study investigates the coupled influence of geometrical curvature and material properties on the flexural capacity of URM walls subjected to out-of-plane loading. Experimental characterization of clay bricks and selected mortar mixes revealed significant variability in elastic stiffness relative to compressive strength, highlighting the heterogeneous nature of masonry materials. These properties were incorporated into a nonlinear finite element model developed in ABAQUS using simplified micro-modelling and traction-separation interface laws, which successfully reproduced crack initiation, stiffness degradation, and ultimate failure mechanisms reported in experimental studies. Parametric analyses showed that planar walls exhibited bending-dominated behaviour governed by tensile cracking, with increased mortar strength improving load capacity without significantly altering failure mode. In contrast, curved walls, as indicated by moment-curvature relationships, developed compressive thrust paths and arching mechanisms that increased stiffness and flexural capacity through stress redistribution and geometric stiffening. An effective section modulus relationship based on wall projection is proposed to estimate the flexural capacity of curved URM walls. The results demonstrate that geometric curvature has a greater influence on out-of-plane flexural capacity than material strength, highlighting the need to incorporate curvature effects into the analysis and design of masonry walls where planar assumptions may underestimate structural performance.

Keywords: Curved Masonry walls, Simplified Micro-Modelling, Out-Of-Plane loads

1. INTRODUCTION

Masonry construction accounts for approximately 70% of the global building inventory (Wang et al., 2018), with Unreinforced Masonry (URM) making up a significant portion of that total (Penner & Elwood, 2016). Its widespread use is not only global but also highly localized, driven by the availability of local materials, low embodied energy, and its reputation as a sustainable construction material (Osorio et al., 2024). Despite this dominance as a construction material, URM remains one of the most vulnerable structural systems, particularly under seismic and extreme weather events. A major weakness lies in out-of-plane (OOP) failure, a recurring cause of structural collapse observed in post-earthquake assessments worldwide (Furtado et al., 2020); (Toshniwal et al., 2024); (Osorio et al., 2024); (Galati et al., 2005). During seismic or storm events, masonry structures are subjected to both in-plane and out-of-plane actions (Noor-E-Khuda et al., 2016). While in-plane shear behaviour has received more extensive research attention as the primary lateral load-resisting mechanism (Tariq et al., 2023), OOP behaviour remains comparatively underexplored despite being an equally critical threat to life safety (Xie et al., 2021). This gap has prompted continued interest in identifying strategies for improving the OOP resistance of URM systems (Li & Zeng, 2023).

Most existing approaches to improving the out-of-plane capacity of masonry walls focus on reinforcement strategies (Fam et al., 2015; Galati et al., 2005, Ram Parajuli & Ghimire, 2021) and enhancements in material properties (Maccarini et al., 2018; Junaid Iqbal, 2021). However, as architectural practice increasingly embraces curved and non-linear forms; modifying wall geometry offers an alternative and relatively underexplored opportunity to augment lateral resistance through architectural form. Traditional construction provides early evidence, with curved wall forms observed in Hakka houses in China, Bhunga dwellings in India, Yomata houses in Malawi, and rammed earth structures in Argentina (Briseghella et al., 2019). Supporting this observation, empirical studies on scaled unreinforced adobe walls reported up to 11% higher lateral resistance in circular configurations compared to square ones Samali et al., (2011) & Jinwuth et al., (2011). However, since curvature was not isolated, the performance gains cannot be attributed solely to it, highlighting the need for systematic investigation. Consequently, despite its apparent advantages and increasing architectural adoption, geometrical curvature remains largely unaccounted for in current design codes and analytical models, signalling a disconnect between architectural ambition and structural design frameworks (Elmorsy et al., 2019).

It is apparent that existing design standards are fundamentally tailored for straight walls and do not capture the complex stress distributions and deformation patterns introduced by curvature, leaving a gap in analytical guidelines for curvilinear masonry walls. While design theories for curved forms such as arches, domes, and curved beams may seem applicable due to geometric similarity, fundamental differences in structural behaviour limit their use. Curved beam theory assumes homogeneous,

isotropic, and linear elastic materials, unlike masonry, which is composite, anisotropic (Šakić et al., 2023), and exhibits nonlinear behaviour from cracking, mortar deterioration, and joint separation (Hejazi & Kaviani Dezaki, 2023). It also assumes small, uniform cross-sections relative to the radius of curvature, whereas masonry walls often have large cross-sections. Similarly, arch theory relies on thrust lines and compressive stability (Huerta, 2006; Rondeaux et al., 2018), and is unsuitable for thin curved URM walls incapable of resisting thrust within the wall thickness (Xie et al., 2021), prone to bending, cracking, and localized failure (Heyman, 1982). Additional limitations include difficulties in quantifying material deterioration and the common assumption of rigid supports, which may not reflect actual boundary conditions (González del Solar et al., 2023; Galati et al., 2005), further highlighting the need for models that capture material nonlinearity and realistic deformation.

This study adopts the flexural design approach, which accounts for masonry's anisotropic behaviour and incorporates geometry through the section modulus. Based on the principle of virtual work, it relates external loads and deflections to internal moments along crack lines and their rotations (Giordano et al., 2017). Flexural capacity, governed by material properties and sectional geometry (Osorio et al., 2024), is captured through ***M-ϕ*** (moment-curvature) relationships developed via finite element simulations. This enables the development of a predictive tool that explicitly quantifies the influence of geometrical curvature on flexural capacity, extending the design scope of existing analytical formulations, rather than relying on crude approximations from seamlessly applying straight-wall models to curved masonry walls.

1.1. Defining geometrical curvature

Curvature is derived from the moment-curvature relationship, which describes a structural element's response to bending moments, influenced by material properties and cross-sectional geometry (Giordano et al., 2017b); in this context, curvature is linked to material strengths (Wilding & Beyer, 2016). In this research study, curvature is defined in terms of the geometrical radius, quantifying the deviation of a wall from a straight-line form before the application of any loads. Unlike traditional definitions that associate curvature with bending behaviour under applied forces, this study treats curvature as an inherent geometric property of the wall. This distinction allows for a clearer examination of how initial geometry influences structural performance, independent of load-induced deformations.

For a uniform curvature(**κ**) is defined as $\boldsymbol{\kappa = 1/R}$; and the relationship between projection, ***h*** with radius of curvature, ***R*** can be approximately expressed in the formula; where in ***c*** which is the shortest distance between two points of a known curve length. From ***Equation 1,*** Yiga et al., (2025), suggests that a larger radius results in a gentler curve with lower curvature, while a smaller radius leads to a sharper, more pronounced curve with higher curvature. Building on this, the fundamental assumption in this study is that a straight wall can be considered a unique curved wall with an infinitely large radius; (**R =**

∞), meaning its curvature is zero. Since curvature measures how much a shape deviates from being straight, a straight line represents the case of no deviation/projection; (**h = 0**). This makes it the least curved shape possible, contrasting with circles or other curves that have a finite radius and allows us to investigate a spectrum of curved walls. For this reason, the validation of the numerical models is based on experimental studies carried out on a straight wall.

$$R = \frac{h}{2} + \frac{c^2}{8h} \qquad (1)$$

The investigation is founded on the following research questions *(a)* In what ways can a validated Finite Element Model, developed from established studies, reliably simulate the out-of-plane response of URM walls? *(b)* To what extent does mortar strength affect the ultimate load-carrying capacity of curved URM walls under out-of-plane loading, as predicted through Finite Element Parametric Analysis? *(c)* How does geometrical curvature, considered independently of other parameters, influence the flexural capacity of URM walls subjected to out-of-plane loads? The corresponding conceptual framework is illustrated in ***Figure 1***

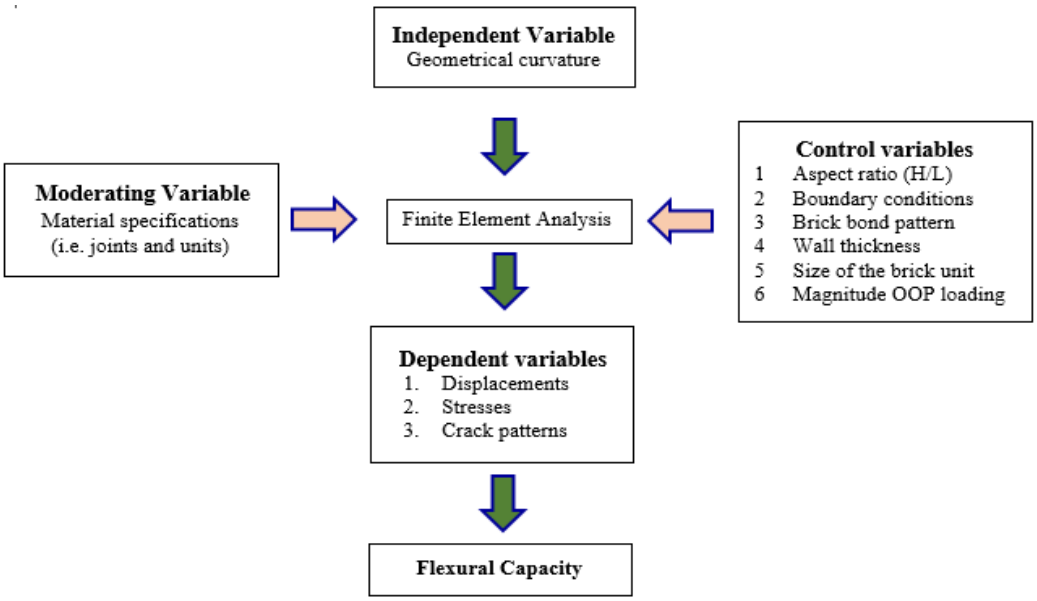


Figure 1: *Conceptual framework for the study*

1.2. Research Objectives

1. To develop a baseline Finite Element Model for URM walls under out-of-plane loading, based on published studies.
2. To analyse the influence of mortar strength on the ultimate load-carrying ability of curved URM walls using Finite Element Parametric Analysis with quantified mechanical properties of masonry constructed derived through laboratory experiments.
3. To evaluate the isolated effect of geometrical curvature on the flexural capacity of URM walls.

1.3. Overview of Numerical Modelling Approaches

This study adopts Finite Element Modelling (FEM) for masonry walls, informed by prior work by (Avasthi & Rai, (2021) and Naciri et al., (2022)on masonry arches, Gentry et al., (2009)'s parametric BIM on doubly-curved walls under vertical loads only, and Abdulla et al., (2017)'s simulation of C-shaped walls, demonstrating FEM's applicability to non-planar geometries. Masonry can be simulated using three main approaches: Macro, Simplified Micro, and Micro Modelling (Milani et al., 2006), as illustrated in ***Figure 2***. The choice of modelling approach depends on the required level of accuracy and detail, with each method offering a trade-off between computational efficiency and the ability to capture intricate masonry behaviour (Maria et al., 2018). Of these, the Simplified Micro-modelling is most promising in simulating masonry at the structural components' level; as it assumes that cracks and frictional slip mainly take place in mortar joints (Chang et al., 2021). In this method, mortar joints are represented as zero-thickness interface elements, while bricks are expanded by half the thickness of the adjacent mortar joint and modelled as solid elements, with the interface elements connecting them (Patel & Dubey, 2022). This approach strikes a balance between computational efficiency and accurate identification of wall crack patterns.

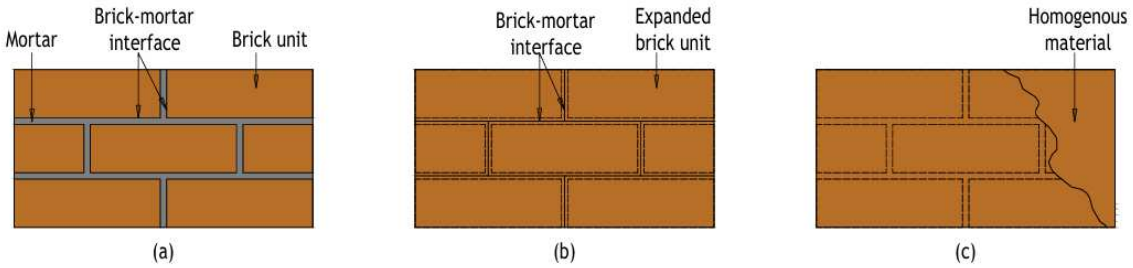


Figure 2*: Finite element modelling approaches: (a) detailed Micro-model; (b) simplified Micro-model; (c) Macro-model*

1.3.1. Modelling approach

Masonry's structural weaknesses stem from its least resistant components and the nature of their interfaces (González del Solar et al., 2023). A key factor influencing its behaviour is the orientation of mortar joints that is to say, bed and head joints, which act as potential planes of failure(Milani et al., 2006). According to (Asteris et al., 2014) the relationship between joint orientation, the directions of the stresses, unit dimensions, and properties dictates the mode of failure, either localized within joints or involving both joints and units.

Regardless of the modelling approach, the successful simulation of masonry's structural behaviour depends critically on both the accurate characterization of material properties (Teschemacher et al., 2023) and the ability to capture its key failure mechanisms (Maria et al., 2018). In line with these requirements, this study employs simplified 3D constitutive models within a simplified micro-

modelling framework, to represent the dominant failure modes observed in masonry structures, namely: (a) joint cracking, (b) sliding along bed or head joints under low normal stress, (c) direct tensile cracking of units, (d) diagonal tension cracking under higher normal stress, and (e) unit splitting due to mortar dilatancy at high stress;(Abdulla et al., 2017)

1.3.1.1. Surface-based cohesive behaviour model

This constitutive model accounts for the linear and fracture behaviour of bed and head mortar joints, considering the traction-separation characteristics between masonry units (Noor-E-Khuda et al., 2016) see ***Figure 3***. The model is based on the plasticity of the dilatant interface capable of simulating the initiation and propagation of interface fracture under combined normal and shear stresses (González del Solar et al., 2023). As a result, key failure modes, including tensile cracking and shear sliding of joints were effectively simulated.

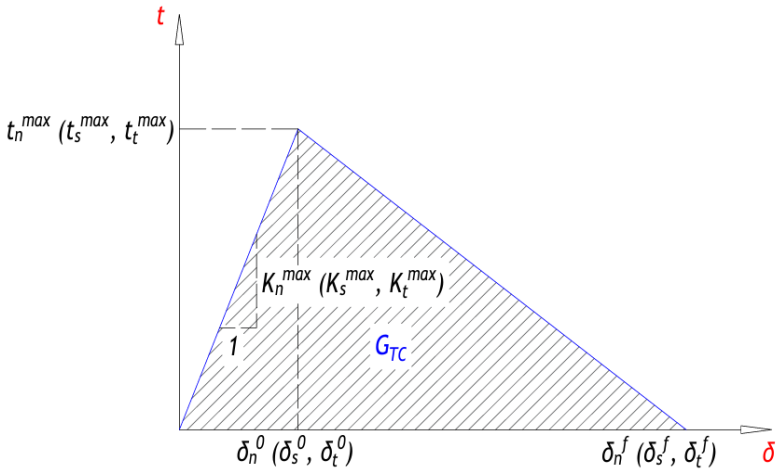


***Figure 3**: Traction separation response of masonry joint interfaces (Abdulla et al., 2017)*

a) Elastic response of the joint interfaces

The initial behaviour of the joint interfaces relies on a linear traction-separation relationship before any damage occurs. This linear behaviour is mathematically represented using an elastic stiffness matrix equation $\boldsymbol{t = K \bullet \delta}$ (Abdulla et al., 2017), relating the directional tractions of the surface, and their corresponding separations *(see **Equation (2)**)*.In the context of a simplified micro-model, which considers interfaces between expanded masonry units, the components of the stiffness matrix, $\boldsymbol{K}$ encompass the stiffnesses of both brick and mortar under identical boundary conditions. Consequently, the equivalent stiffness coefficients for these joint interfaces are expressed as functions of the elastic moduli of both the mortar and the masonry unit, and the thickness of the mortar joint (Milani et al., 2006) as shown in ***Equations (3)** and **(4)**.*Where $\boldsymbol{G_u}$ and $\boldsymbol{G_m}$ are the brick-unit shear modulus and mortar joint shear modulus, respectively (MPa), $\boldsymbol{h_m}$ is mortar thickness (mm), $\boldsymbol{E_u}$ and $\boldsymbol{E_m}$ are elastic moduli of masonry brick units and mortar (MPa), respectively.

$$\boldsymbol{t} = \begin{Bmatrix} t_n \\ t_s \\ t_t \end{Bmatrix} = \begin{bmatrix} K_{nn} & 0 & 0 \\ 0 & K_{ss} & 0 \\ 0 & 0 & K_{tt} \end{bmatrix} \begin{Bmatrix} \delta_n \\ \delta_s \\ \delta_t \end{Bmatrix} = \boldsymbol{K}\,\boldsymbol{\delta} \qquad (2)$$

$$K_{nn} = \frac{E_u E_m}{h_m\,(E_u - E_m)} \qquad (3)$$

$$K_{ss} = K_{tt} = \frac{G_u G_m}{h_m\,(G_u - G_m)} \qquad (4)$$

b) Plastic response of the joint interfaces

The initiation of damage in masonry joints, marked by crack propagation, follows the quadratic traction criterion. This criterion is satisfied when the quadratic sum of the stress ratios at the masonry interfaces reaches a value of one, as formulated by (Campilho et al., 2008) - see ***Equation (5)***

$$\left(\frac{t_n}{t_n^{max}}\right)^2 + \left(\frac{t_s}{t_s^{max}}\right)^2 + \left(\frac{t_t}{t_t^{max}}\right)^2 = 1 \qquad (5)$$

Once this threshold is reached, crack propagation commences, signifying the onset of damage. The evolution of this damage is not abrupt but is instead governed by the dissipation of fracture energy, with the dissipated energy per unit area, (G_f) (Patel & Dubey, 2022), playing a crucial role in the process.

The quadratic traction criterion models damage evolution through a fracture energy approach, ensuring progressive rather than abrupt failure. Its effectiveness lies in predicting damage initiation at masonry joint interfaces, particularly under mixed-mode loading. The critical mixed-mode fracture energy dissipation, $\boldsymbol{G_{TC}}$ (N/mm), is derived from the Benzeggagh-Kenane (BK) law (Benzeggagh, 1996), which is applicable when the fracture energies in both shear modes (Mode **II** and Mode **III**) are similar, a characteristic of masonry joints.

To model the softening behaviour that follows damage initiation, different approaches can be used depending on the failure mode considered. Softening may be linear (Pantò et al., 2017), bilinear (Vaculik & Griffith, 2017), or exponential (Chang et al., 2021). In this study, a linear softening law was adopted, capturing the gradual degradation of the mortar joints- see ***Figure 3*****.** This model accurately simulates progressive crack growth, allowing the joint interface to maintain some residual strength before complete separation.

In addition to progressive tensile cracking, the plastic response of masonry joints must also account for shear-driven failures. Finally, defining the tensile strength of brick wall connections to assess their

tendency to crack under tension, the critical shear stress τ_{crit} at which a joint fails, as described by the Mohr-Coulomb criterion, is a relationship between the cohesion at brick joints c (MPa), the frictional coefficient between brick joints; μ, and σ_n is the normal contact pressure stress at the brick joint interfaces (MPa); expressed in ***Equation (6)***.

$$\tau_{crit} = c + \mu\sigma_n \qquad (6)$$

1.3.1.2. Elastic behaviour of expanded units

To ensure an equivalent elastic response between the expanded masonry units and the original masonry assemblage (i.e., comprising both units and mortar), it is necessary to adjust the elastic modulus of the expanded units (Milani et al., 2006). This adjustment is a function of the moduli of elasticity of the original masonry units and mortar, and the geometric characteristics of the masonry assemblage. Several researchers have proposed equations for this purpose, assuming a stack bond between masonry units and uniform stress distribution within the masonry constituents. For simplicity with the variables, ***Equation (7)*** by (González del Solar et al., 2023) shall be adopted in the proposed study.

$$\boldsymbol{E_{adj}} = \frac{HE_u E_j}{nh_u E_j + (n-1)h_j E_u} \qquad (7)$$

1.3.1.3. Drucker-Prager plasticity model

This is employed to simulate the non-linear response of masonry units under compressive loading conditions. This model accommodates both isotropic hardening and softening behaviours, enabling the simulation of potential compressive failures in masonry structures (Alejano & Bobet, 2012). The DP plasticity model is parametrically defined to account for both linear and non-linear deformations. Within the linear criterion, key parameters such as flow stress ratio, dilation angle, and friction angle must be precisely specified, while the evolution of the yield surface during nonlinear deformations is determined by the uniaxial compression plastic behaviour characteristic of the masonry assemblage.

2. METHODOLOGY

A combined experimental and numerical approach was employed to investigate URM wall flexural behavior. Mechanical properties of locally made clay bricks and mortars were experimentally determined and integrated into a validated ABAQUS Finite Element model. Parametric analyses assessed the influence of mortar strength and geometrical curvature on ultimate out-of-plane capacity. Curved walls of varying radii were simulated, while experimental masonry prisms provided benchmark validation through load-deflection responses and crack pattern comparison, ensuring the model accurately captured failure mechanisms.

2.1. Laboratory experimentation

A total of 150 clay bricks (200×110×100mm) were procured from Kawanda and selected via preliminary quality checks, including soundness, hardness, structural integrity, and impact resistance, which confirmed uniform, crack-free, and durable bricks. Randomized sampling captured natural variability, while maintaining a constant brick type ensured that differences in masonry prism strength reflected only variations in mortar composition. To assess compressive mortar strength per BS EN 1015-11, (100×100×100mm) cubes were prepared for four mix classes; **M12** (1:0:3), **M6** (1: ½:4½), **M4** (1:1:6), and **M2** (1:2:9), designed in accordance with BS 5628-Part1 (1992). A constant water-to-cement ratio of 0.4 was maintained. Tororo Portland Pozzolana Cement (CEM IV B(P) 32.5N) and hydrated lime served as binders. A total of **12** specimen, three (3) for each of the four mortar mixes, were demoulded after 24hours, and cured in water for 28days. Masonry prisms consisted of three vertically stacked bricks with 10mm mortar joints (see ***Figure 4)***, reaching approximately 350mm height, limited by the Universal Testing Machine. Prisms were built on level bases and left undisturbed until testing. While 28-day curing is standard, it was omitted to avoid shrinkage-related weakening of the mortar-brick bond. Three prisms per mix were tested, totalling 12 assemblages.



Figure 4*: Preparation of brick prisms for laboratory experiments*

The prisms were tested under uniaxial compression in accordance with ASTM C1314-09 (2011). Compressive strength tests were performed on individual bricks, brick prisms, and mortar cubes using a 1000kN capacity Universal Testing Machine, following the procedures in BS EN 772-1 (see ***Figure 5).*** The compressive stress for each specimen was calculated by dividing the applied load by the net cross-sectional area. Strain measurements were obtained using a dial indicator attached to the specimen with steel straps and bolts. tests were conducted at **Energo Projekt Test laboratory** along Kampala-Gulu Highway in Kawanda in Uganda

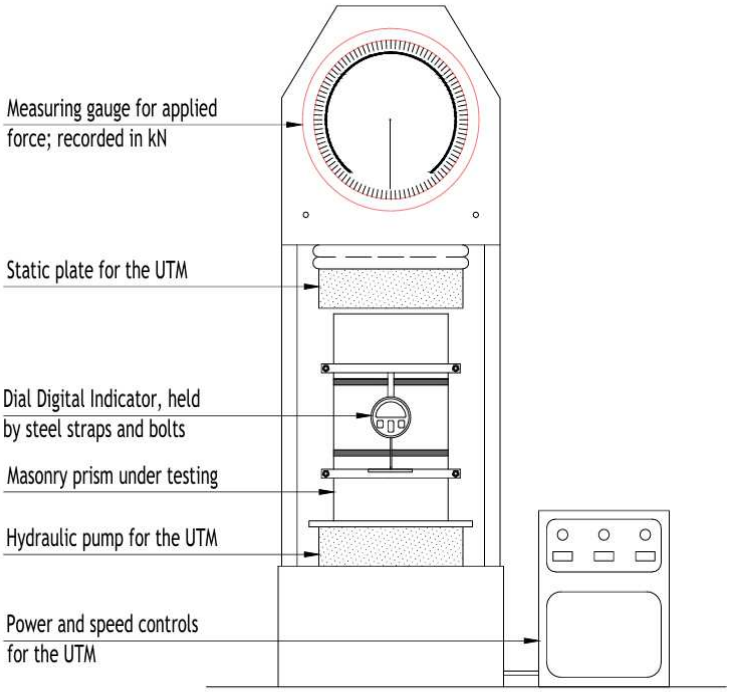


***Figure 5**: Apparatus setup for the Compressive strength tests*

The height-to-thickness, h_p/t_p ratio for each prism was calculated using its height and the least lateral dimension. A correction factor was determined from ***Table 1*** of ASTM C1314-09, (2011) and applied to the calculated ratio, thereby normalizing the compressive strength results across prisms with varying slenderness ratios, ensuring that reported values more accurately reflect the true material strength rather than geometric influences. The stress-strain curves of masonry obtained were idealized using six limit states, i.e., $0.33f'_m$, $0.75f'_m$, $0.90f'_m$, f'_m, $0.5f'_m$, and $0.2f'_m$, which correspond to significant stages of material response (Kaushik et al., 2007b). The corresponding elastic moduli of the specimen were derived from stress-strain curves by calculating the secant slope between **5%** and **33%** of the specimen's ultimate compressive strength (Kaushik et al., 2007a). The experimental procedure was designed to determine the elastic moduli of individual masonry units and masonry prisms. Upon establishing these values, a derived analytical expression, ***Equation (8)*** from (Vermeltfoort et al., 2007), was employed to estimate the elastic modulus of the mortar joints, based on the composite behaviour of the prism, an output essential for the derivation of equivalent stiffness coefficients for the joint interfaces, as defined in Equations ***(3)*** and ***(4);*** where h_j denotes the height of the mortar joint, h_u is the height of the masonry unit, E_m represents the elastic modulus of the masonry assemblage, E_j is the elastic modulus of the mortar joint, and E_u is the elastic modulus of the masonry unit.

$$\frac{h_j}{E_j} = \frac{h_j + h_u}{E_m} - \frac{h_u}{E_u} \qquad (8)$$

2.2. Development of the numerical model in ABAQUS software.

The finite element models were developed using ABAQUS CAE Software. A 3D Simplified Micro-Modelling approach. The development of the numerical models is discussed in the subsections that follow. In addressing the **Specific Objective 1**, a straight wall with geometric masonry conforming to the experimental setup by Vaculik & Griffith, (2017) was adopted. It consisted of a **4.0m × 2.5m** primary web wall with **two** 0.45m × 2.5m return walls (flanges). The wall thickness was 110mm, and the bond pattern followed a half-overlap stretcher bond- see ***Figure 6.***

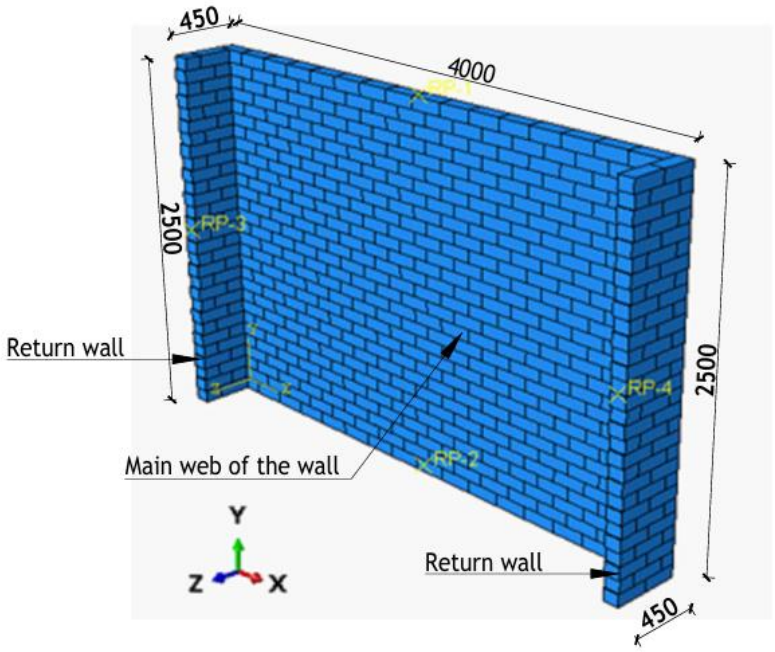
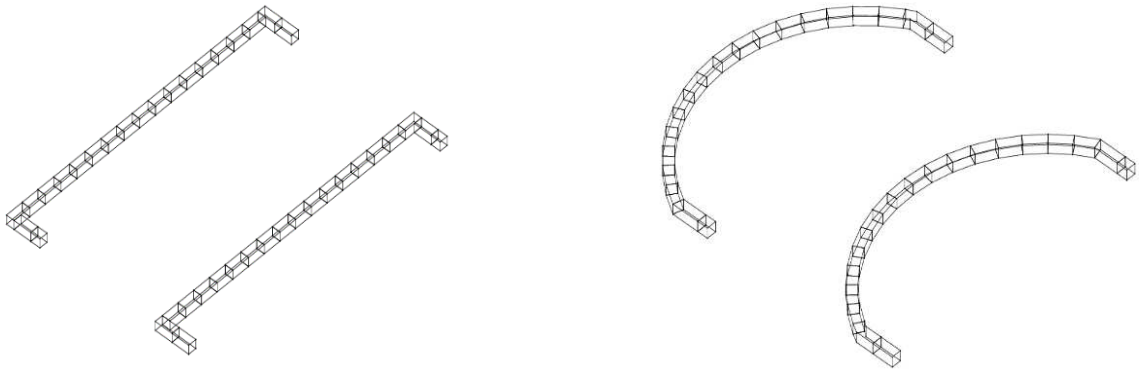


Figure 6*: Geometry of the C-shaped straight masonry wall based on Vaculik & Griffith, (2017)*

The modelling involved creating expanded brick units, adjusting dimensions to account for the 10mm-thick mortar joints. A 2D AutoCAD plan arranged the units in stacked courses, which were then extruded to form 3D objects- see ***Figure 7***. The model was exported as a ***.sat file*** and imported into ABAQUS, with each course added individually. The same approach was applied for geometrically curved walls to maintain consistency in the finite element setup. In ABAQUS, the key surfaces of the bricks were defined to facilitate their identification and proper assembly within the model.



(a) ***(b)***

***Figure** 7: Extruded clay brick parts exported into ABAQUS environment*

***(a)** for the straight wall, **(b)** for the 750mm- projection curved wall*

Each of the expanded brick units was assigned material properties based on literature from experimental studies. Refer to ***Table 2*** for the material properties. These expanded bricks were then stacked in two aligned courses, avoiding overclosure issues. Instances were set as mesh-dependent to streamline meshing, avoiding computational inefficiency from individual meshing. Using a linear pattern, the two-course setup was systematically replicated to form 29 alternating courses, completing the masonry wall assembly.

***Table 2**: Material properties for the masonry units*

Category	**Parameter**	**Value**	**Data Source**
Elastic behaviour of masonry units	Density	1,900kgm^3	Estimated
	E_b	52,700MPa	(Vaculik & Griffith, 2017)
	E_j	420MPa	
	Poisson's ratio	0.15	Assumed
Onset Plastic behaviour (Drucker Prager model)	Friction angle	36°	(D. C. Drucker, 1952)
	Flow stress ratio	1.0	Assumed
	Dilation angle	10°	(Misir & Yucel, 2023)
Hardening behaviour of masonry units	Stress-strain compression curve	see ***Figure 8***	(Kaushik et al., 2007b)
Damage assessment (Quads damage criterion)	Fracture energy	0.08N/mm	(Abdulla et al., 2017) For mode-dependent stress components using the **BK** law (Benzeggagh M, 1996)
	Tensile strength	1.18MPa	(Vaculik & Griffith, 2017)
	Shear strength	1.65MPa	Assumed to be 40% higher than the tensile strength

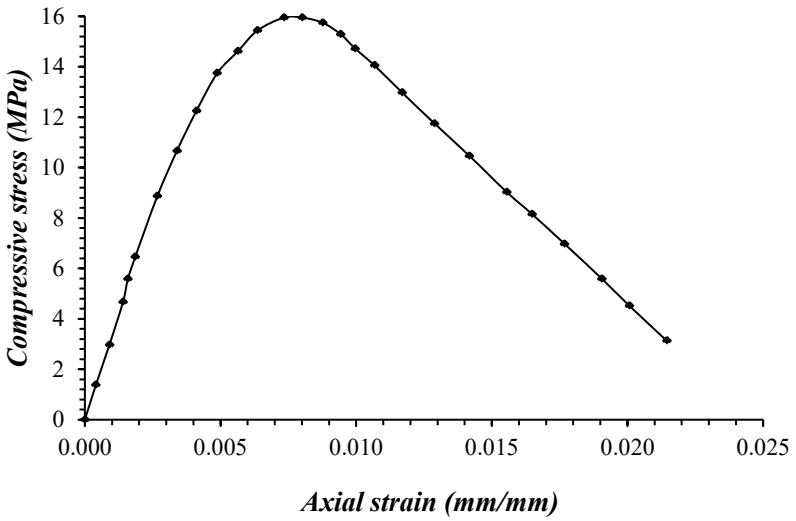


***Figure 8**: Stress-strain compression curve for the masonry wall (Kaushik et al., 2007b)*

The ABAQUS/Standard solver was used for the analysis, suitable for static and quasi-static problems. Out-of-plane loads were applied gradually over a 1-second step, serving as a numerical tool to improve convergence without dynamic effects. A general nonlinear static procedure accounted for material nonlinearity, geometric deformations, and contact interactions. Automatic increment control was employed, with an initial increment of 0.001 and limits from 1E-55 to 1, allowing accurate resolution of highly nonlinear behaviour. The Direct equation solver provided exact solutions for the large system of equations generated by the SMM approach. The Full Newton-Raphson method iteratively updated the stiffness matrix to achieve equilibrium at each increment. No artificial damping was used, ensuring realistic wall behaviour. The load application followed a linear ramp from 0 to 100%, preventing sudden force jumps and numerical instability. Default symmetric matrix storage optimized memory, while automatic increment control enabled the solver to adjust step sizes for stability.

Interaction properties between the expanded brick units were assigned to model the mortar joints. Contact formulations, including normal and tangential behaviour, were applied to simulate bonding and potential failure mechanisms between bed-joint surfaces of masonry units. The traction-separation law was used to define interface behaviour. The contact interaction property parameters used are shown in ***Table 3.*** The contact interactions between adjacent masonry units were modelled using a node-to-surface discretization with finite sliding. Top and bottom surfaces, representing bed joints, were assigned distinct contact properties, as torsional failure of bed joints is the predominant failure mode compared to head joints (Chang et al., 2021). Tangential behaviour followed a penalty friction formulation, while normal behaviour employed a hard contact model to prevent penetration and tensile stress transfer (Bolhassani et al., 2015). Interface damage was governed by the Quadratic Traction Criterion with linear softening and energy-based evolution (Vaculik & Griffith, 2017), stabilized with a viscosity coefficient of 0.002 (Abdulla et al., 2017). Boundary supports used a kinematic coupling

approach, assigning reference points as master nodes with six degrees of freedom constrained, while surfaces served as slaves. The coupling radius extended to the outer boundary, ensuring interaction, and was applied to all four wall planes: top, bottom, and the two return faces, totalling four constraints.

***Table 3**: Material properties for the joint interfaces*

Failure behaviour	Parameter	Value	Data Source
Tangential behaviour	Friction coefficient	0.75	Estimated
	Shear stress limit (i.e. cohesion)	0.04MPa	(Maria et al., 2018)
Normal behaviour	Contact pressure-overclosure relationship	-	Hard contact behaviour (Bolhassani et al., 2015)
Cohesive behaviour (Stiffness coefficients)	K_{nn}	42N/mm^3	Calculated from Equations (2) and (3) (Milani et al., 2006).
	K_{ss}	17N/mm^3	
	K_{tt}	17N/mm^3	
Damage assessment (quadratic stress criterion)	Fracture energy	0.012N/mm	(Vaculik & Griffith, 2017)
	Maximum normal stress (tension)	0.12MPa	(Milani et al., 2006).
	Maximum nominal stress (shear)	0.17MPa	(Milani et al., 2006).
	Viscosity coefficient	0.002	(Abdulla et al., 2017).

A quasi-static lateral load of 5kPa with a ramp amplitude for smooth load introduction was applied to the wall's outer web, excluding a uniform area of two-brick courses near supports. The support boundary conditions were defined under the mechanical category in the *initial step* and propagated to *Step 1*. All constraint boundary conditions were implemented as simple supports applied at designated control nodes (reference points), which serve as reference points for enforcing the constraints. The expanded masonry units were modelled using eight-node 3D hexahedral (C3D8R) elements with reduced integration to improve computational efficiency and default hourglass control to prevent numerical instabilities. Default parameters for viscosity, distortion control, element deletion, and maximum degradation were retained. A 5×2×2 mesh was chosen based on a mesh sensitivity study by (Abdulla et al., 2017)

The final analysis involved running ABAQUS CAE simulations to examine displacement fields, stress distributions, and failure mechanisms of the masonry wall. Reaction forces at defined reference points were aggregated and divided by the loaded web area to determine applied pressures, excluding top and bottom return wall forces due to geometric inconsistencies. Out-of-plane displacements at the wall centre were plotted against applied pressure to produce force-displacement curves. Model validation compared these curves and assessed crack initiation, propagation, and failure patterns using the maximum principal stress criterion. Quantitative validation employed Root Mean Square Error

(RMSE), Mean Absolute Error (MAE), normalized RMSE (NRMSE), Pearson correlation (r), and area between curves to ensure close agreement with experimental results.

2.3. Parametric numerical analysis of the curved walls constructed with local materials

Parametric studies examined the influence of wall curvature and mortar class by varying wall projections from 250mm to 1000mm (see ***Figure 9)***, with corresponding radii calculated from a predefined relationship given in *Equation 1*. Wall height and length were fixed at 2.5m and 4m, respectively, to isolate curvature effects, while bonding patterns, return wall sizes, and boundary conditions remained constant. Material properties, including density, elastic modulus, and plastic strain evolution, were derived from laboratory tests and used in the Drucker-Prager model. Default interface and mortar parameters were retained to align with the validated model. This analysis quantified how mortar strength and geometrical curvature affect the flexural capacity and overall structural performance of masonry walls, addressing ***Specific Objective No. 2***. and ***3.***

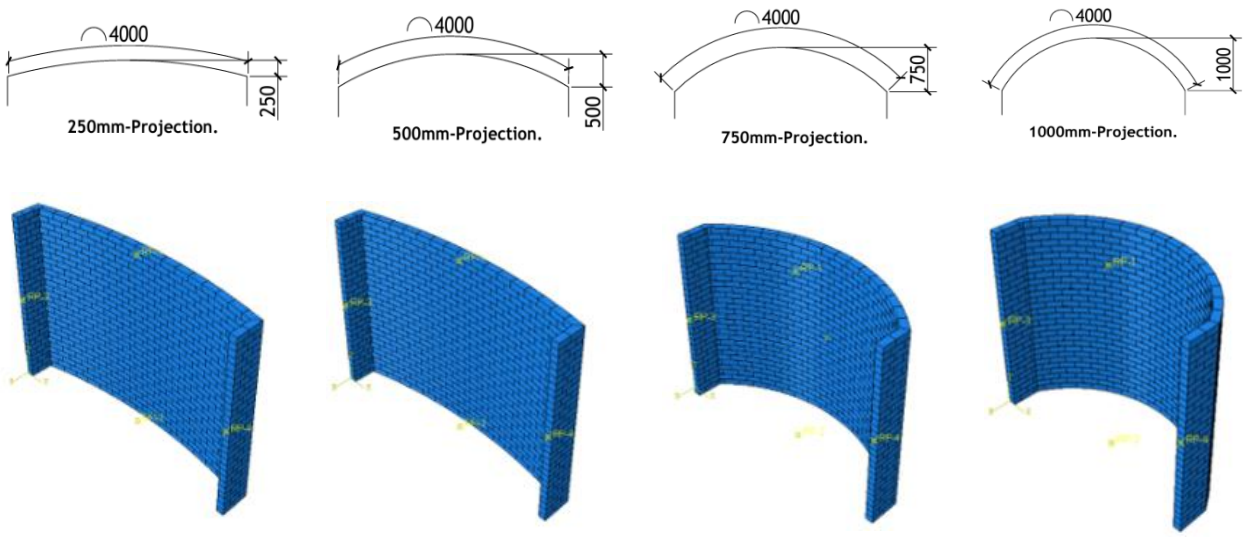


Figure 9*: Selected models of masonry walls for numerical analysis (Yiga et al., 2025)*

2.4.Procedure for Constructing the Moment-Curvature Relationship

In the SMM models developed, C3D8R elements were used in this study for their ability to capture complex three-dimensional stress states. However, unlike beam or shell elements, they do not directly provide internal section moments (Simulia, 2014). Therefore, to estimate the bending moments within the wall, the analysis turned to classical structural mechanics, with the walls subjected to uniform lateral pressure with simple supports under symmetric loading, the internal moment at mid-span was derived indirectly from reaction forces; from the formula, $M = (q \times h^2) / 8$, where q represents the intensity of the lateral pressure load, and h is the height of the wall. Moment capacity along planes perpendicular to the bed joints was not considered, as it is consistently higher than along the parallel planes. Failure

was considered most likely along planes parallel to the bed joints, which are more susceptible in a two-way bending mechanism (Arya, 2022), and this informed the assessment approach.

Curvature, being a derivative of rotation along the wall height, was estimated using a displacement-based approximation (Godio & Beyer, 2019). Since curvature is not a direct output from the numerical models, it was computed by measuring the horizontal displacement difference ***(Δu)*** between two nodes located along a vertical X-plane cut at the mid-span of the wall; one at the top edge and the other at mid-height. The vertical distance between these nodes was approximately half the wall height. Assuming this displacement occurs uniformly over the wall height and across its full thickness, based on (Cavaleri et al., 2009) the curvature ϕ was calculated using the expression $\phi = \Delta u / (t \times x)$, where t is the wall thickness (which is also the distance between the tension and compression faces), and x is the vertical height over which rotation occurs (taken as approximately 0.5 × wall height depending on the measurement points).- see ***Figure 10***

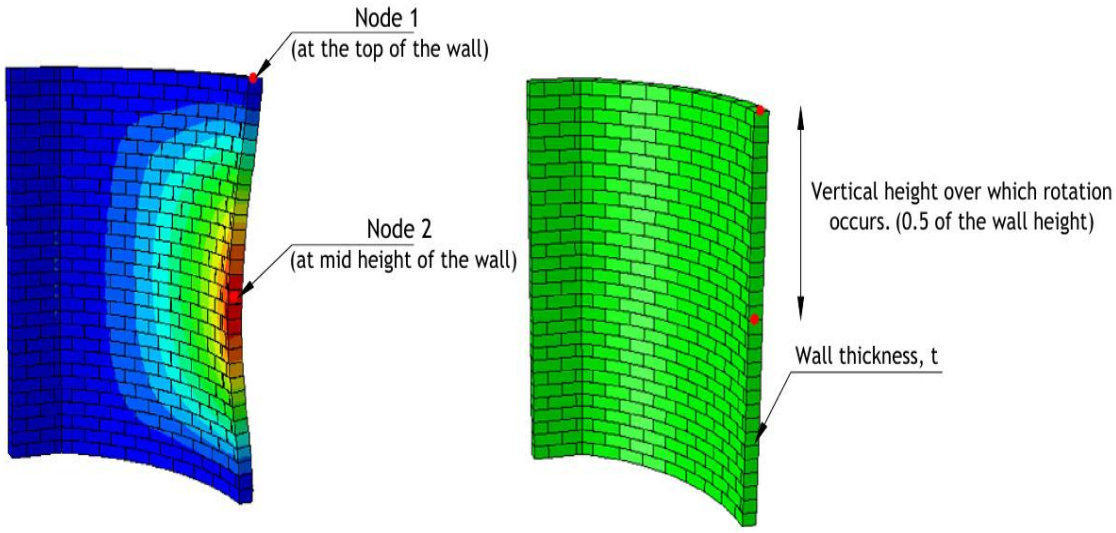


Figure 10*: Vertical X-plane cut for Derivation of Moment-curvature relations for a URM wall*

During post-processing, the required data for moment and curvature calculations was extracted from ABAQUS. History outputs for reaction forces *(RF3)* and displacements *(U3)* were recorded at selected nodes and reference points. These values were then combined using the previously described expressions for M and ϕ, calculated at each time increment. The results were exported to Microsoft Excel, where they were processed to generate a continuous moment-curvature curve, capturing the wall's flexural response from initial loading through peak capacity and into the post-peak regime.

3. RESULTS AND DISCUSSION

3.1. Laboratory Test Results

With **Specific Objective 2** in addressing the research question**:** *How do the mechanical properties of masonry constructed using locally sourced bricks and mortar vary, and to what extent do these properties influence structural behaviour?* The results of compressive tests conducted on the mortar cubes were used to produce the stress-strain curves presented below. A total of 12 specimens were tested, with each mortar mix represented by three specimens. The results were used to develop the stress-stain relationship of the mortar cubes, presented in ***Figure 11.*** The summary of the results is presented in ***Table 3.***

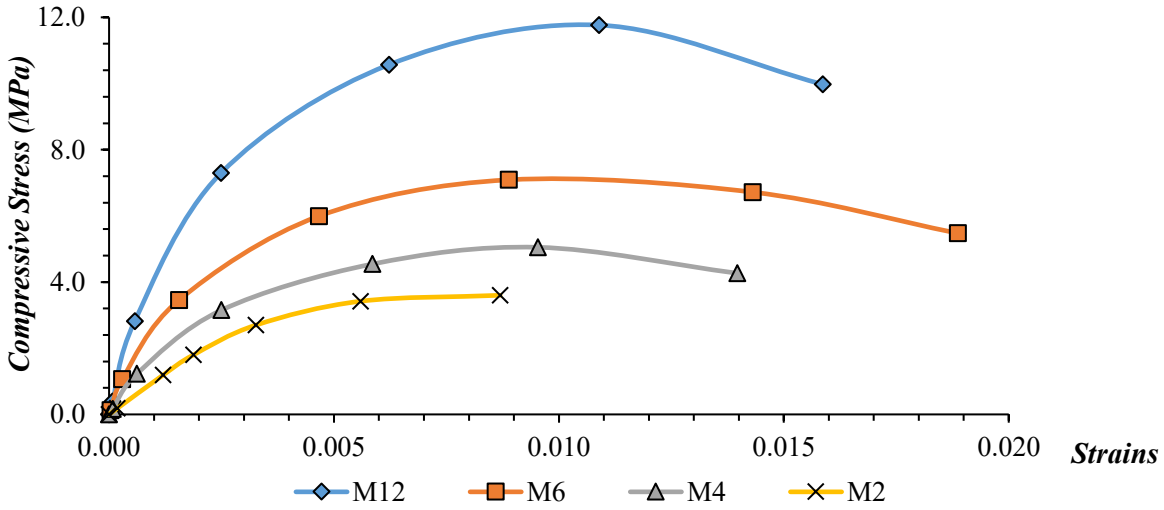


Figure 11*: Stress-Strain curves for Mortar cubes*

Table 3: *The Compressive strengths and the Elastic moduli of the Mortar cubes.*

Mortar type	No. of tests	Compressive strength (MPa)		Elastic Modulus (MPa)	
		Standard dev.	Mean	Standard dev.	Mean
M2 (1:2:9)	3	0.10	3.42 (0.03)	83.70	1182.01 (0.08)
M4 (1:1:6)	3	0.32	5.13 (0.06)	268.15	2002.92 (0.13)
M6 (1: ½:4½)	3	1.05	6.72 (0.16)	151.22	3630.00 (0.04)
M12 (1:0:3)	3	0.25	11.76 (0.02)	1039.68	5051.36 (0.21)

Coefficient of variance (CoV(%)) has been written in parentheses

The stress-strain curves in ***Figure 11*** demonstrate a theoretically consistent and structurally relevant trend: increasing mortar strength enhances both the compressive strength and elastic modulus of masonry prisms. This is driven by the densification of the cementitious matrix (Giordano et al., 2017) and the refinement of the interfacial transition zone (ITZ) between mortar and brick units (Freiherrova & Krejsa, 2019). With higher cement content, particularly evident in the shift from M2 to M12, the

reduction in porosity and increase in particle packing improve not only material strength but also interfacial cohesion, resulting in more integrated load transfer mechanisms (Gumaste et al., 2007). However, strength introduces a critical trade-off. Stronger mortars exhibit brittle fracture characteristics, with steep post-peak declines in stress-strain responses. This is a consequence of their low fracture energy and limited plastic deformation capacity (Huang et al., 2020). In contrast, lower-strength mortars such as M2, while structurally weaker, possess greater ductility and strain accommodation capacity.

Figure 12 illustrates the compressive stress-strain behaviour of three masonry unit samples, along with an average curve. The details of these experimental results are summarised in ***Table 4.*** The clay bricks exhibited substantial variability, with elastic stiffness showing a coefficient of variation up to 77%, the highest recorded among tested specimens. This pronounced scatter reflects the inherent non-uniformity of locally produced units, even from the same kiln or production batch. Contributing factors include inconsistent firing, heterogeneous clay composition, and microstructural defects, which also affect compressive strength. Such variability underscores the necessity of accounting for material heterogeneity in both experimental investigations and numerical simulations, as localized anomalies can disproportionately influence global wall behaviour. These findings highlight the critical importance of stringent quality control during brick production to ensure reliable structural performance. For numerical modelling, an average stress-strain curve was adopted to provide a representative response, smoothing out sample-to-sample fluctuations and yielding an average compressive strength of 4.5MPa.

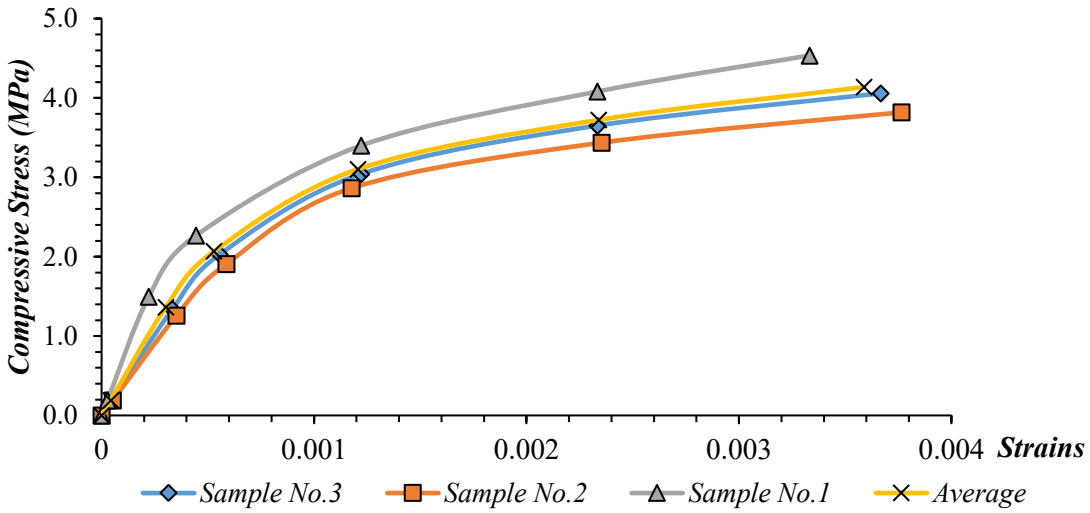


Figure 12*: Stress-Strain curves for the masonry brick units*

Table 4: *Summary of the mechanical properties for the brick units*

Specimen	No. of tests	f_b (MPa)	E_u (MPa)	Density (kg/m)	Dimensions (mm)
Clay bricks	3	4.14 (0.09)	3579.84 (0.77)	1583	200×110×100

Coefficient of variance (CoV (%)) has been written in parentheses

The compressive tests conducted on the masonry prisms yielded the stress-strain curves presented in ***Figure 13*** to ***Figure 16***. The results showed that stress redistribution in masonry prisms produced a composite response, with stiffness and compressive strength values between those of the brittle bricks and more ductile mortar. Prisms with higher-strength mortar carried higher compressive loads but showed lower ultimate strains, likely due to reduced micro-cracking and interface movement. Stronger mortar improved load transfer and structural rigidity, but also resulted in a more brittle failure mode.

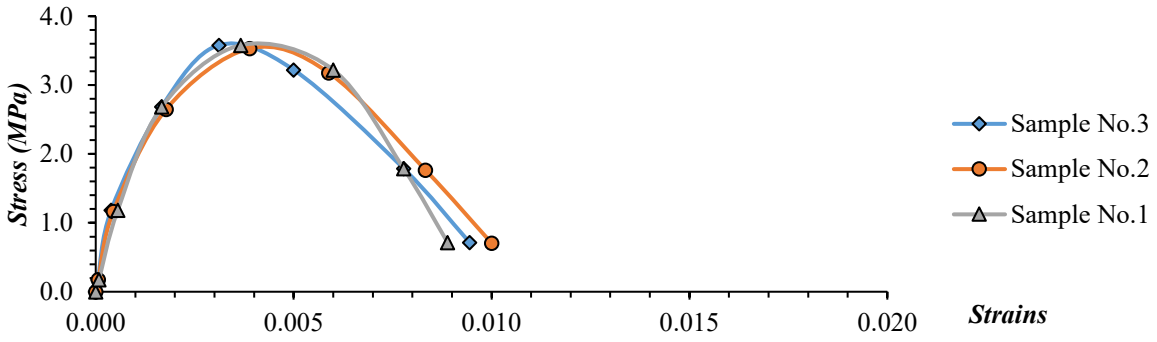


Figure 13: *Stress-Strain curves for three M12 Mortar mix masonry prisms*

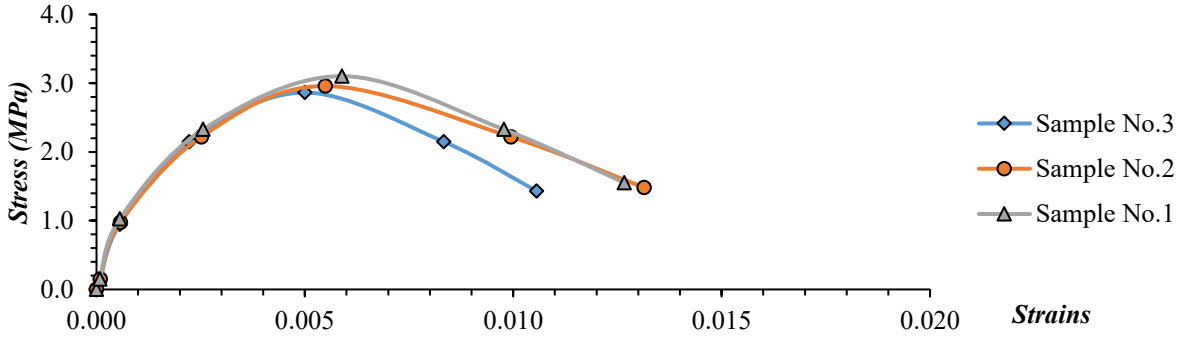


Figure 14: *Stress-Strain curves for three M6 Mortar mix masonry prisms*

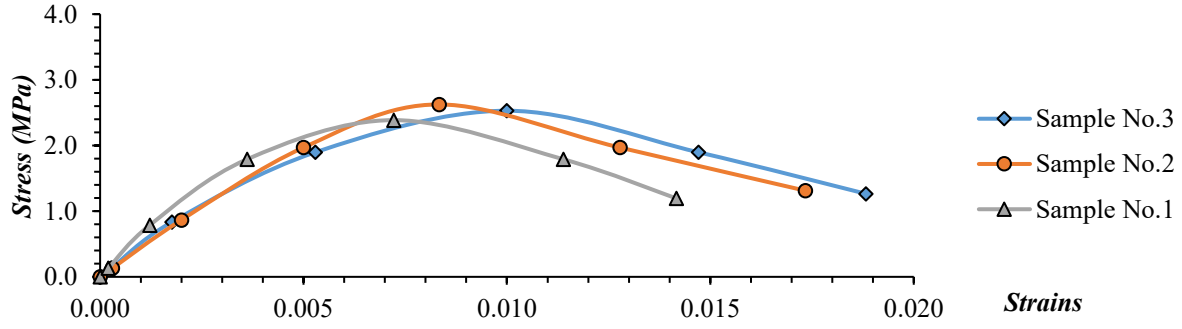


Figure 15: *Stress-Strain curves for three M4 Mortar mix masonry prisms*

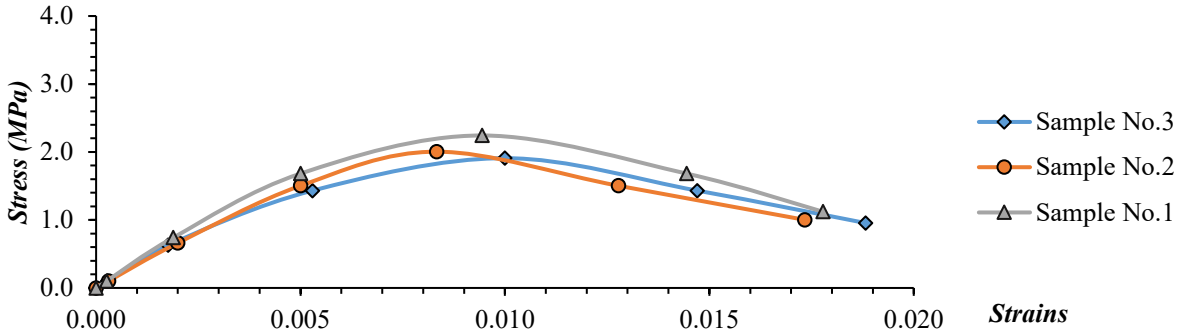


***Figure 16**: Stress-Strain curves for three M2 Mortar mix masonry prisms*

The variability in results changed with mortar strength. For compressive strength, the coefficient of variation decreased from 7% for M2 mortar to 1% for M12, indicating stronger mortars produced more consistent peak loads due to improved mortar uniformity and composite action. In contrast, the elastic modulus variability increased from 9% to 18%, suggesting stronger mortars amplified scatter in stiffness, likely due to their brittle nature and sensitivity to brick-mortar bond imperfections. This shows that stronger mortars improve strength but increase uncertainty in elastic behaviour- see ***Table 5***.

***Table 5:** The Compressive strengths and the Elastic moduli of the masonry prisms.*

Mortar type	No. of tests	Compressive strength (MPa)		Elastic Modulus (MPa)	
		Standard dev.	Mean	Standard dev.	Mean
M2 prism	3	0.14	2.08 (0.07)	30.68	359.88 (0.09)
M4 prism	3	0.12	2.51 (0.05)	112.20	516.82 (0.21)
M6 prism	3	0.12	2.98 (0.04)	79.66	1750.88 (0.05)
M12 prism	3	0.03	3.56 (0.01)	456.22	2595.38 (0.18)

Coefficient of variance (CoV(%)) has been written in parentheses

As a general trend across all specimens, compressive strength exhibited lower variability than elastic modulus, reflecting a more uniform peak load response across samples (Nazimi et al., 2024). Strength is governed by the ultimate crushing of the brick-mortar assemblage, which is relatively insensitive to micro-defects, whereas the elastic modulus depends on early-stage deformation mechanisms, microcrack opening, pore interactions, and interface stiffness, highly sensitive to firing, clay composition, moisture, and workmanship (Vermeltfoort et al., 2007). Even with higher-strength mortars, modulus scatter persists due to microstructural heterogeneity and differential interface stiffness, underscoring why stiffness-based predictions require stricter quality control and more conservative assumptions.

3.1.1. Equivalent stiffness coefficients for mortar

The elastic modulus of the mortar joints within the brick prism was determined using ***Equation (8)***. Based on ***Equations (3)*** and ***(4)***, the equivalent stiffness coefficients for the mortar-brick interfaces were subsequently derived. These coefficients are functions of the elastic moduli of the mortar and brick units obtained from laboratory testing. The calculated values are presented in ***Table 6***

Table 6: *Elastic Moduli and Equivalent Stiffness Coefficients of Mortar Joints for Each Mix*

Mortar type	(E_m) (MPa)	(E_j) (MPa)	K_{nn} (N/mm^3)	K_{ss} / K_{tt} (N/mm^3)
M2 (1:2:9)	359.88	45.93	4.65	2.02
M4 (1:1:6)	516.82	68.88	7.02	3.05
M6 (1: ½:4½)	1750.88	358.57	39.85	17.33
M12 (1:0:3)	2595.38	839.92	109.74	47.71

The exponential rise in normal interface stiffness (K_{nn}) with mortar strength, as shown in ***Figure 17***, stems from more than just matrix densification. As mortar grades increase from M2 to M12, the microstructure becomes finer, with reduced voids, better particle packing, and stronger hydration bonds (Schneemayer et al., 2014). These developments enhance both adhesion and friction at the brick-mortar interface, causing a sharper, nonlinear gain in resistance to tensile separation (Hernoune et al., 2025). K_{nn} increases disproportionately due to the elevated crack initiation thresholds and improved bond mechanics (Li & Zeng, 2023). In contrast, the increase in shear stiffness (K_{ss}/K_{tt}) is less pronounced and remains significantly lower than K_{nn} across all mortar grades. This disparity occurs because shear resistance at the interface is governed primarily by surface roughness, cohesion, and friction rather than compressive strength alone (Debnath et al., 2023; Shadlou et al., 2020). As a result, sliding along the interface may still initiate early even in high-strength mortars, limiting substantial gains in shear stiffness. Improving shear performance, therefore, requires modification of the interface itself, such as increasing surface roughness, introducing mechanical interlock, or providing bed-joint reinforcement to enhance shear transfer. Overall, the greater sensitivity of K_{nn} compared to K_{ss} indicates that out-of-plane flexural behaviour is governed more by resistance to tensile opening than by shear transfer, explaining the strong influence of mortar strength on flexural capacity.

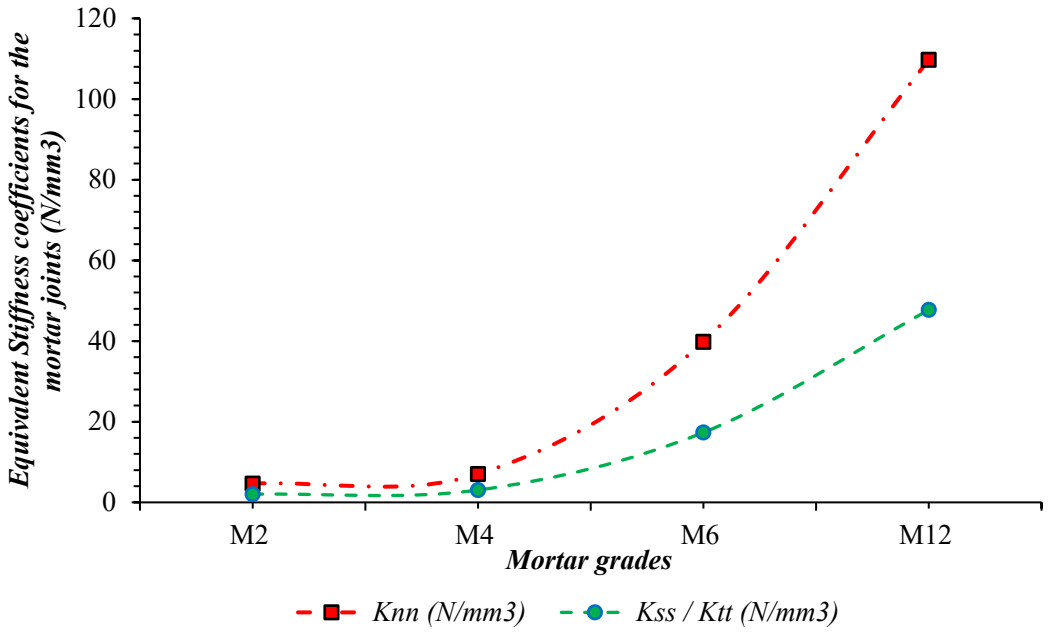


***Figure 17**: Evolution of the equivalent stiffness coefficient values across mortar designations*

3.2.Validation of the numerical model for the Straight Wall

In **Specific Objective 1** aimed to address the research question: *In what ways can a validated Finite Element Model, developed from established studies, reliably simulate the out-of-plane response of URM walls?* A straight wall FE model was developed to closely replicate the behaviour of the actual C-shaped wall studied by Vaculik & Griffith. This alignment was essential to validate the model before it was used for the parametric analysis of curved URM walls, constructed from local materials. Quantitatively, the validation results in ***Figure 18*** indicate that the numerical model exhibits a strong agreement with the experimental data. The Root Mean Square Error (**RMSE**) of 0.31 kPa reflects a small average deviation between predicted and measured pressures, while the Mean Absolute Error (**MAE**) of 0.26kPa indicates that the typical point-to-point discrepancy is minimal. The Pearson correlation coefficient (***r***) of 94.5% confirms a very strong similarity in curve shape, demonstrating that the model effectively captures the experimental response trend. The Normalized RMSE (**NRMSE**), corresponding to only 10% of the total pressure range, indicates that the errors are small relative to the magnitude of the response. Additionally, the area between curves, measured at 6.89kPa·mm, represents the cumulative difference across the full displacement range and remains limited, further supporting the overall fidelity of the simulation. These metrics demonstrate that the model predicts the experimental response with high reliability, and the small errors observed fall well within acceptable engineering limits.

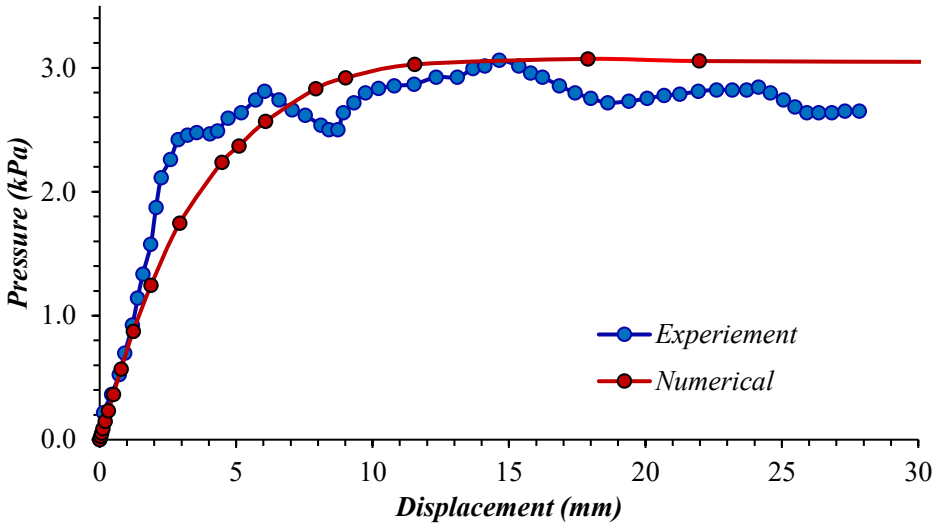
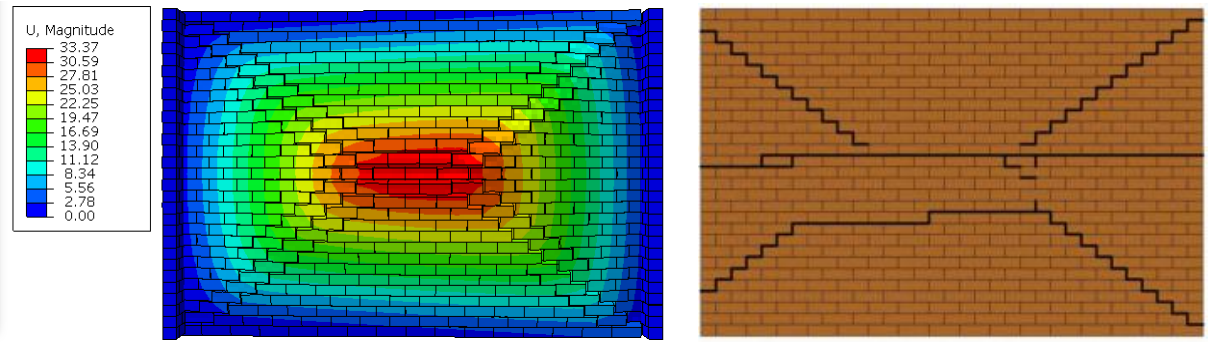


***Figure 18**: Relationship between applied pressure and displacement of the web section of the wall.*

While pressure-displacement curves capture the global structural response, they do not represent localized behaviours such as crack initiation, hinge formation, and non-uniform displacement fields (Godio & Beyer, 2019). The observed patterns confirmed that the model reproduced both load capacity and failure mechanisms (***Figure 19a***). In the experimental study by Vaculik & Griffith, (2017), failure involved horizontal cracking at mid-height on the inner wall with stepped diagonal cracks toward the corners (***Figure 19b***). The numerical model reproduced a similar pattern, though with more distributed diagonal cracking, likely due to estimated material properties and the assumption of uniform unit-mortar interface properties (Abdulla et al., 2017), which overlooks the likely variability in joint strength caused by workmanship, material quality, and localized stress concentrations (Plevris & Asteris, 2014).



(a) ***(b)***

***Figure 19**: Comparison of the crack patterns of the (a) Developed a numerical model against (b) the Experimental by Vaculik & Griffith, (2017)*

The moment-curvature (***M-ϕ***) relationship is a key indicator of flexural behaviour in masonry walls under out-of-plane loading and was used here for further model validation. The simulation-derived ***M-ϕ*** curve in ***Figure 20*** for a straight wall was compared with analytical models by Cavaleri et al., (2009)

and Noor-E-Khuda et al., (2016). All models showed similar elastic stiffness and predicted a peak moment of about 2.4kNm, with divergence lying not in strength prediction, but in post-peak behaviour. The FE model exhibited a plateau response, likely due to modelling choices that limit damage evolution, while the analytical models showed softening, a more realistic post-yield. Despite this difference, the FE model accurately predicts peak moment capacity and overall flexural response, indicating that it is sufficiently reliable for evaluating out-of-plane flexural behaviour in masonry walls.

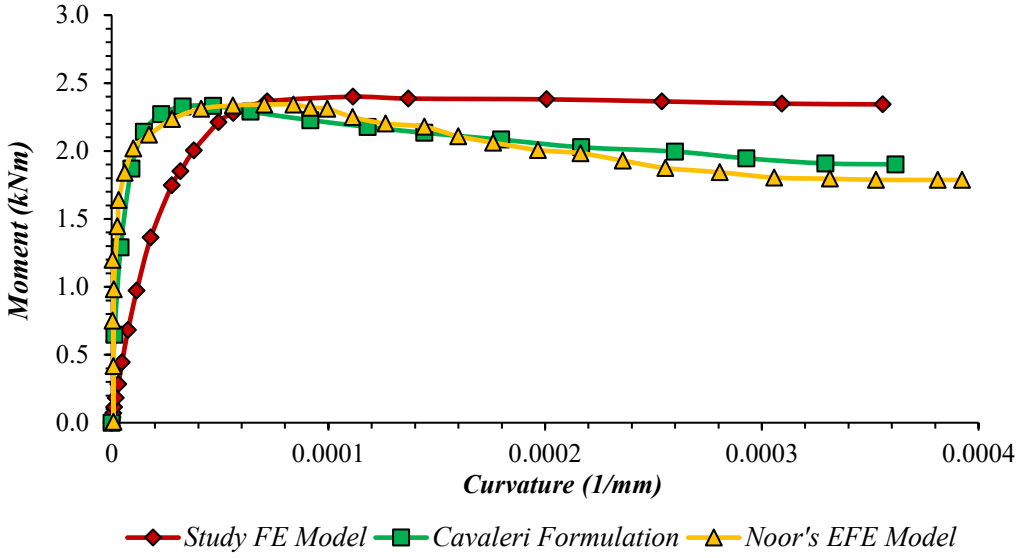


Figure 20: *Moment-curvature relation for the validation study*

3.3. Parametric numerical analysis

3.3.1. Effect of mortar strength on the ultimate resistance of curved URM walls

In addressing ***Specific Objective 2*** and the associated research question: *To what extent does mortar strength affect the ultimate load-carrying capacity of curved URM walls under out-of-plane loading, as predicted through Finite Element parametric analysis?* A parametric study was conducted using the selected numerical models of curved masonry walls. The models incorporated material properties derived from laboratory experiments. Four levels of wall curvature were considered, represented by wall projections of 250 mm, 500 mm, 750 mm, and 1000 mm, along with a straight wall datum (0 mm projection). Each curvature was analysed across four mortar grades: M2, M4, M6, and M12. The results of this parametric study are presented in ***Figure 21*** to ***Figure 25***.

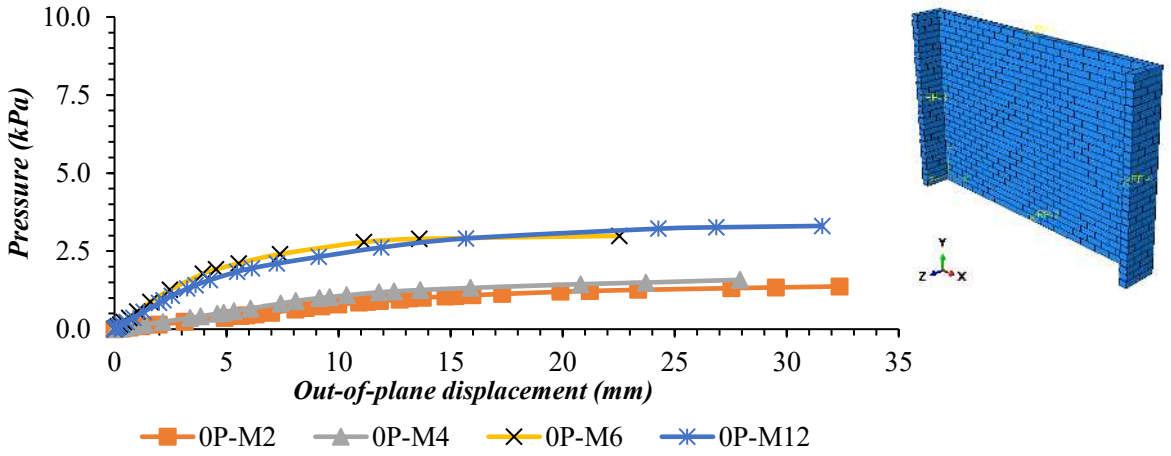


***Figure 21**: Pressure-displacement capacities curves for the 0mm-projection curved walls*

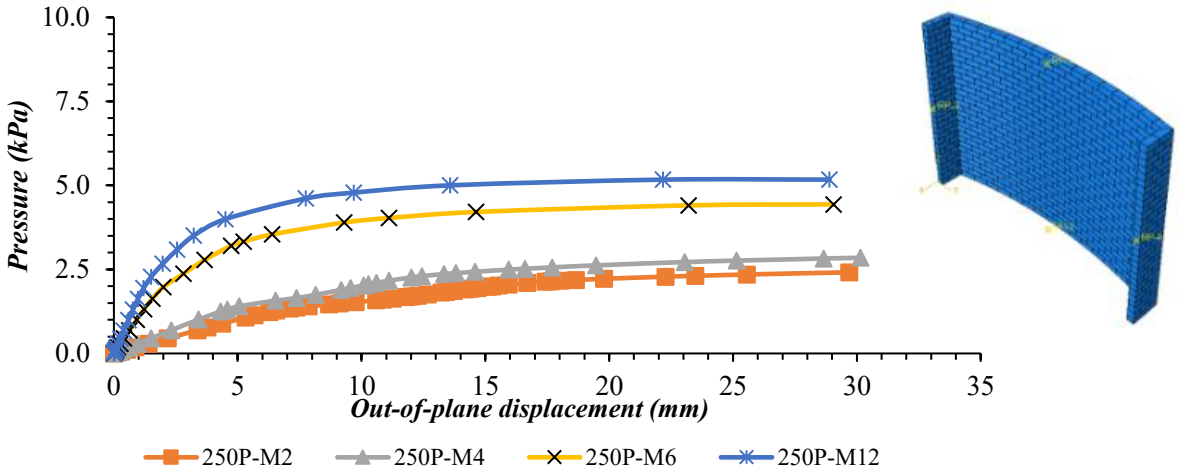


***Figure 22**: Pressure-displacement capacities curves for the 250mm-projection curved walls*

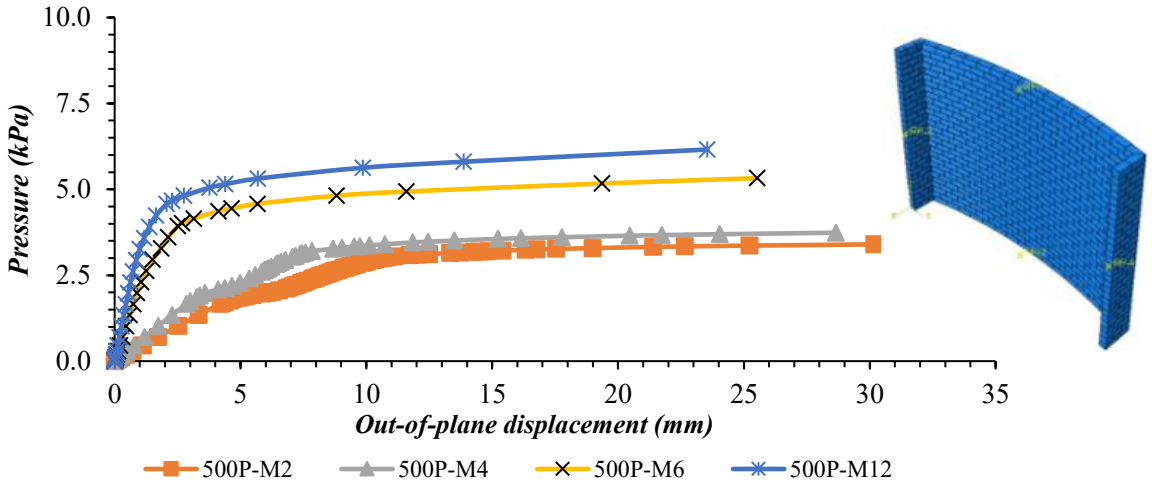


***Figure 23**: Pressure-displacement capacities curves for the 500mm-projection curved walls*

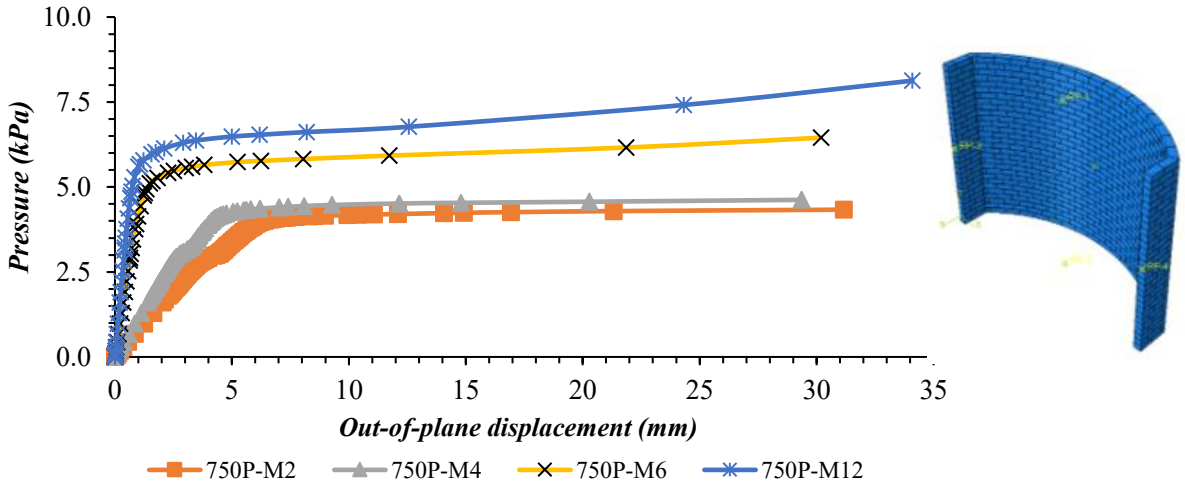


***Figure 24**: Pressure-displacement capacities curves for the 750mm-projection curved walls*

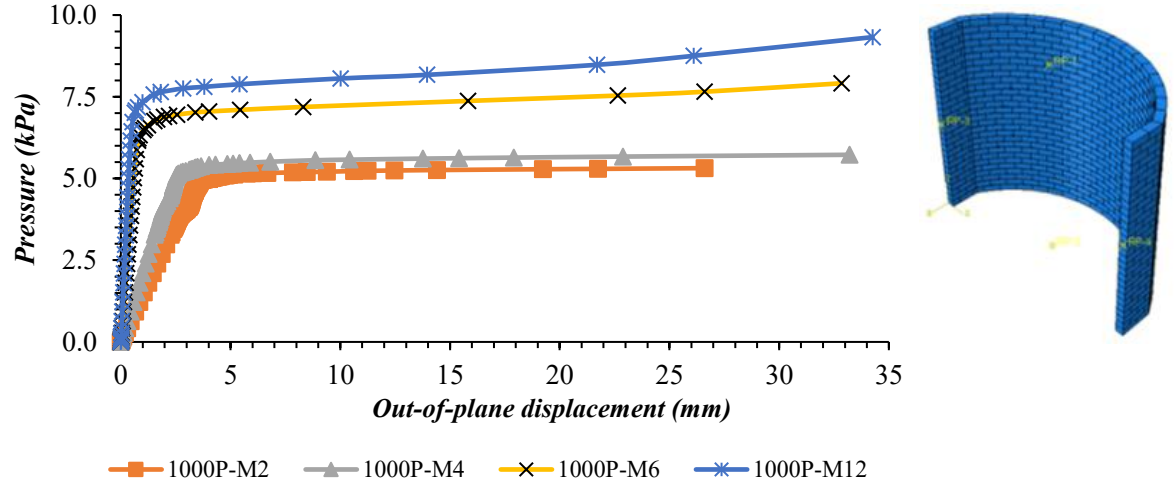


***Figure 25**: Pressure-displacement capacities curves for the 1000mm-projection curved walls*

Across all wall configurations (see ***Figure 21*** to ***Figure 25***), mortar strength and wall curvature jointly govern load capacity and failure behaviour through distinct mechanical mechanisms. In walls with weaker mortars (M2, M4), early joint compression and interface slip occur because the brick-mortar interface yields at relatively low stress. This permits gradual microcrack initiation and propagation along joints before significant stresses develop in the bricks, resulting in lower stiffness and peak loads, but greater ductility and a smoother post-peak response due to distributed cracking and energy dissipation.

As mortar strength increases (M6, M12), the interfaces resist early crushing and sliding, promoting more monolithic behaviour. This enables the mobilization of higher compressive and bending stresses within the masonry, increasing stiffness and peak load capacity. However, because less energy is dissipated through joint slip, cracking localizes more rapidly once tensile limits are reached, leading to a more brittle failure response.

Geometry further modifies this behaviour by altering force transmission. In flat walls, out-of-plane loads are resisted primarily through bending, inducing tensile stresses that must be transferred across the brick-mortar interface. Consequently, mortar strength plays a critical role in maintaining composite action. For flat walls, peak pressures increase from approximately 1.2kPa to 3.0kPa which is a 150% increase, whereas highly curved walls increase from about 5.0kPa to 9.5kPa corresponding to a 90% increase, indicating a stronger dependence on mortar strength. However, flat walls reach a capacity limit governed by brick tensile cracking and compressive crushing, beyond which further increases in mortar strength have a limited effect (see ***Figure 21***)

3.3.2. Influence of Wall Curvature on Flexural Capacity

In addressing ***Specific Objective 3*** and the associated research question: *How does geometrical curvature, considered independently of other parameters, influence the flexural capacity of URM walls subjected to out-of-plane loads?* To evaluate the effect of geometrical curvature on the flexural capacity of unreinforced masonry (URM) walls, moment-curvature relationships were examined for four mortar types (M2, M4, M6, M12). Mortar properties were kept constant while wall curvature increased across five scenarios: straight, 250mm, 500mm, 750mm, and 1000mm projections. Results are shown in ***Figure 26*** to ***Figure 29.***

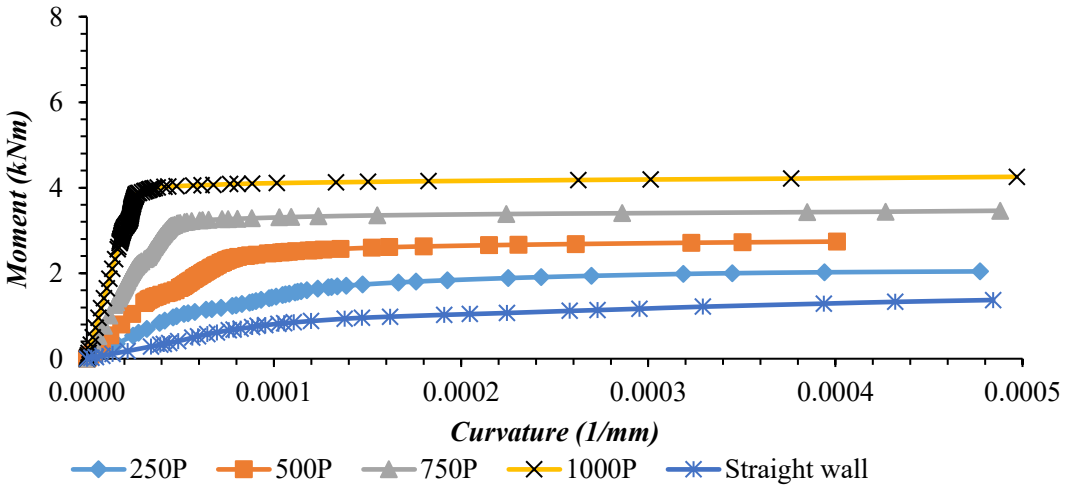


Figure 26*: Moment-curvature relationships for M2 mortar*

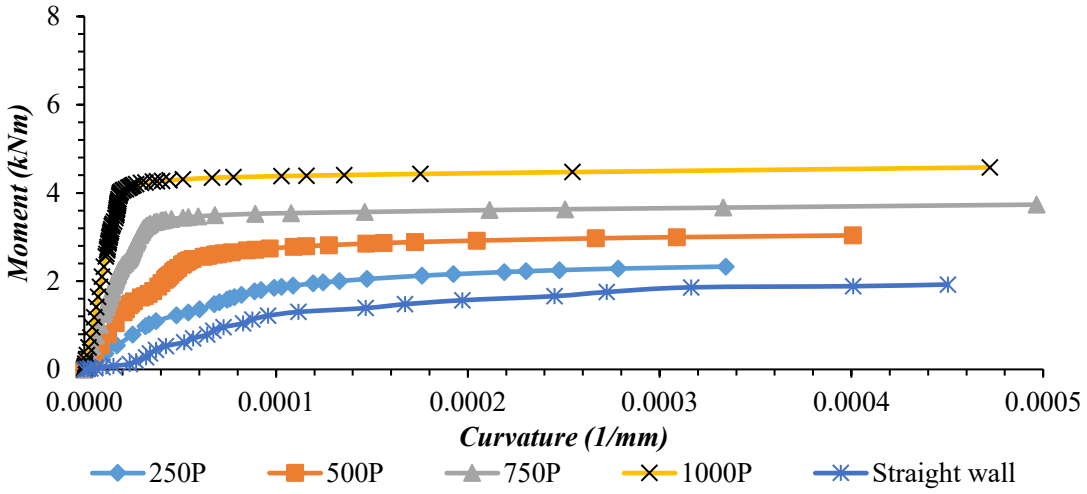


***Figure 27**: Moment-curvature relationships for M4 mortar*

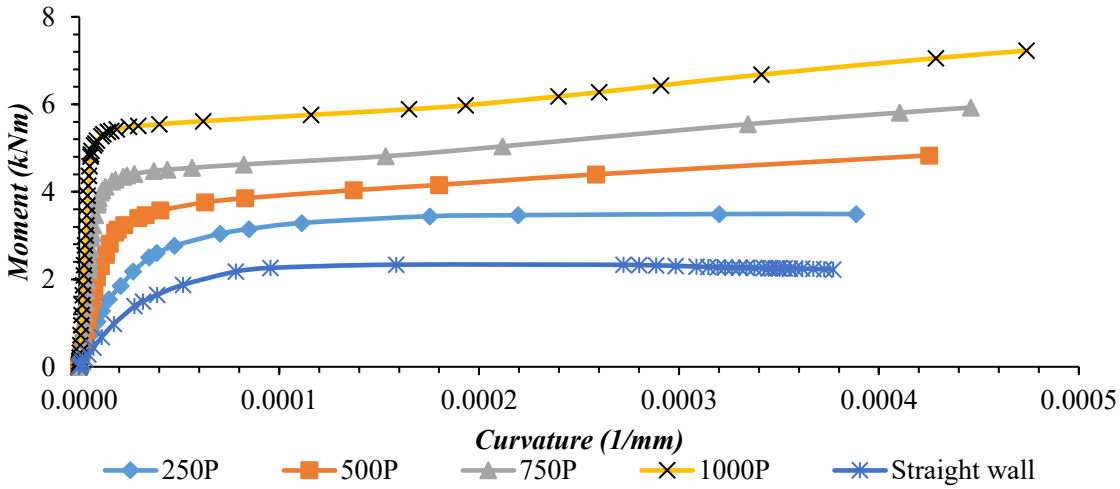


***Figure 28**: Moment-curvature relationships for M6 mortar*

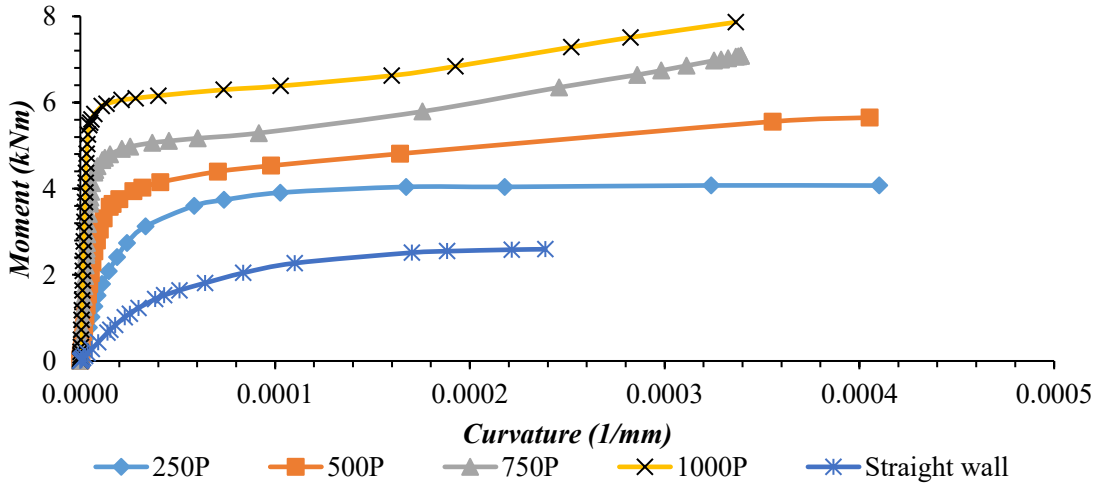


***Figure 29**: Moment-curvature relationships for M12 mortar*

The results show that increasing wall projection consistently enhances moment capacity at yield across all mortar grades, highlighting the combined influence of geometry and material properties. For M2 mortar, the straight wall moment was 0.88kNm, rising 94% at 250 mm and 352% at 1000 mm. M4 mortar increased from 1.3kNm by 46% and 226%, respectively. Higher-strength mortars (M6, M12) exhibit smaller relative gains from curvature; 27% and 65% at 250 mm, and 149% and 167% at 1000mm, while still achieving higher absolute capacities than weaker mortars. Incremental gains for stronger mortars stabilize, indicating that additional curvature contributes proportionally less to relative improvement, though absolute performance continues to increase. The introduction of wall curvature consistently enhances flexural capacity, producing the largest relative gains for weaker mortars, while stronger mortars achieve the highest absolute moment capacities.

This analysis reveals that geometric curvature alters stress distribution in URM walls, inducing arching that generates compressive thrusts along the convex face while reducing tension on the opposite face (Rondeaux et al., 2018). This mechanism enlarges the bending lever arm, mobilizing masonry stiffness and enhancing out-of-plane capacity, even for lower-strength mortars. Curvature also redistributes cracks, delays localization, and improves energy dissipation. Numerical and experimental results show that increasing wall projection or decreasing radius systematically enhances stress engagement, toughness, and post-peak ductility, highlighting curvature as a key parameter governing flexural performance beyond mortar strength (Vermeltfoort et al., 2007).

3.3.3. Estimation of section modulus for the URM walls

The section modulus at cracking was determined by identifying the flexural cracking moment, defined as the point where the moment-curvature (***M-ϕ***) curve deviates from its initial linear path, indicating the onset of tension cracking in the extreme fibre, and dividing the cracking moment by the corresponding maximum principal tensile stress recorded at that step from the corresponding finite element models.

The results in ***Figure 30*** and ***Figure 31*** indicate that the effective section modulus of masonry walls is largely insensitive to mortar grade, with all types converging at each projection. For straight walls, predictions closely align with classical bending theory, confirming both the accuracy of the numerical model and the dominant influence of cross-sectional geometry on flexural resistance. Introducing curvature produces an exponential increase in the section modulus as projection rises, enabling the section to engage additional resisting depth and causing its behaviour to transition from flat-plate bending toward a shell-like response. With an $\mathbf{R^2}$ of 0.96, (***Figure 31***) geometrical curvature, here represented by projection, clearly governs this enhancement, highlighting that classical bending formulas underestimate the flexural capacity of curved masonry walls.

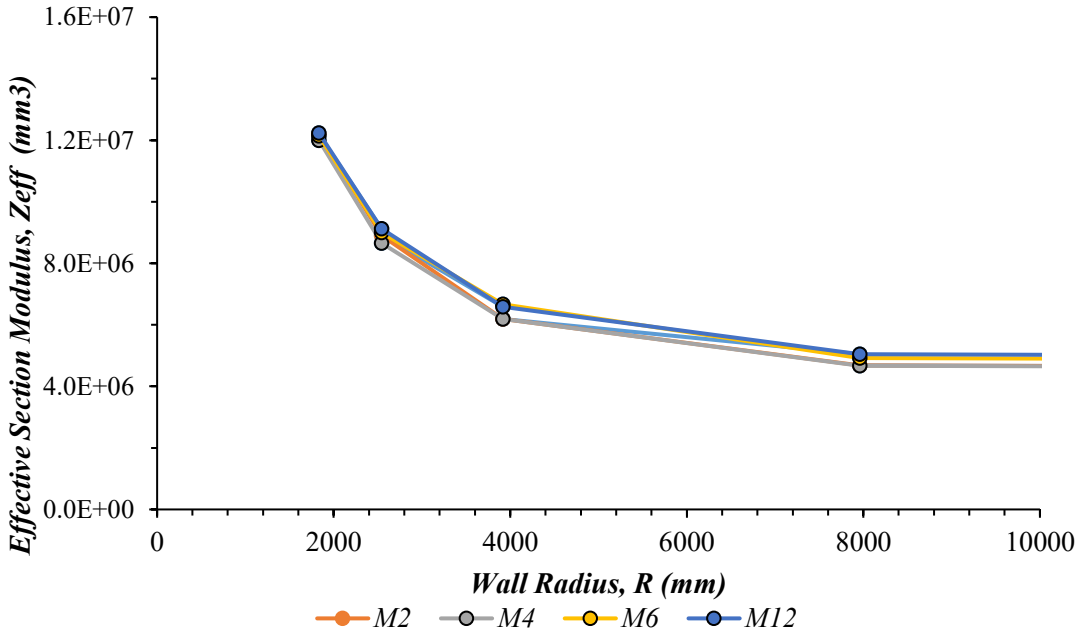


***Figure 30**: Relationship between the section modulus and the wall radius*

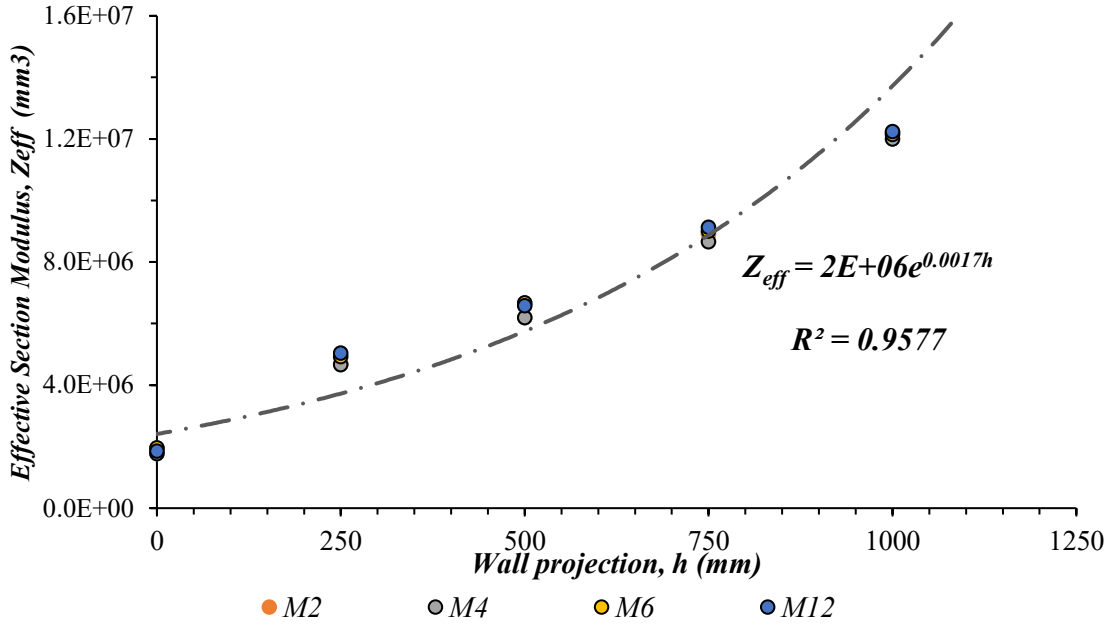


***Figure 31**: Relationship between the section modulus and the wall projection*

The flexural performance of unreinforced masonry (URM) walls subjected to out-of-plane loads is traditionally evaluated using plate theory, where the section modulus **(*Z*)** is a key geometric parameter governing resistance to bending. For planar walls, the classical elastic section modulus is defined as: $Z=bt^2/6$; where ***b*** is the wall width (i.e. per run meter) and *t* is the wall thickness. This formulation assumes linear stress distribution and neglects any contribution from in-plane actions, making it valid primarily for flat plates. In this study effective section modulus **(Z_{eff})**, is not computed from cross-

sectional geometry, but rather derived from numerical simulation; defined from the moment-curvature relationship: $Z_{eff} = M_{cr} / f_{cr}$. Here, M_{cr} is the applied moment at initial cracking, and f_{cr} is the corresponding tensile stress at the extreme fibre. Z_{eff} thus is an approximation of the wall's overall bending capacity, incorporating any nonlinear effects or geometric stiffening present at the onset of cracking, rather than a purely geometric parameter.

For planar walls, the extracted values of Z_{eff} consistently approximate $\mathbf{2\times10^6\ mm^3}$ regardless of the mortar grade, aligning closely with values from the formula $Z=bt^2/6$ obtained from classical theory for a considered wall thickness h=110mm and a width b = 1000mm. This agreement across all mortar types confirms that material strength differences do not significantly influence global flexural stiffness in planar URM walls(Vermeltfoort et al., 2007). It also serves as a validation benchmark for the accuracy of the numerical model in capturing conventional flexural behaviour. However, for curved walls**,** a significant departure from the planar wall behaviour is observed, Z_{eff} increases markedly with decreasing radius of geometric curvature. For instance, at $R \approx 1600$mm, Z_{eff} reaches 1.2×10^7 mm³**,** which is approximately six times the planar value. As the radius increases toward 8000mm, Z_{eff} drops back toward 4.5×10^6 mm³**,** suggesting a gradual return to classical (analytic) values for planar walls (Rondeaux et al., 2018). A similar trend emerges when projection distance **(h)** is used instead of the wall radius, Z_{eff} grows exponentially with projection, following the trend:

$$Z_{eff} = 2\times10^6 e^{0.0017h} = (bt^2/6) \times e^{0.0017h}$$

Where t is the wall thickness, b is taken as 1000mm-width for an equivalent straight wall, and h represents the wall projection; a descriptor of the geometrical curvature for convex URM walls with a uniform radius. Larger projection distances enhance the flexural resistance of curved URM walls not by improving material properties, but by increasing the effective lever arm and enabling the formation of compressive thrust lines; a behaviour not captured by classical plate theory. As a result, the traditional view of section modulus as a fixed, purely geometric property becomes insufficient for describing curved masonry behaviour. Trends in the effective section modulus, Z_{eff} reflect a fundamental shift in load-resisting mechanisms, which, while shell-like in appearance, do not satisfy the assumptions of classical shell mechanics. True shell theory requires thin, continuous materials capable of mobilizing dominant in-plane membrane stresses, whereas masonry is thick, heterogeneous, and brittle, with responses dominated by bending, localized arching, and brick-mortar interface interactions. Cracking, discontinuities, and limited tensile capacity prevent the development of continuous membrane action, so curved URM walls cannot be treated as shells. Consequently, their out-of-plane behaviour must be interpreted through bending-dominated masonry mechanics, and the derived formula provides a physically grounded and practical tool for predicting their flexural resistance

4. CONCLUSION

This study demonstrates that the out-of-plane flexural performance of curved unreinforced masonry (URM) walls is governed more by geometric configuration than by material strength. The application of Simplified Micro-Modelling, combined with moment–curvature relationships, validates the methodology in the extraction of an effective section modulus (*Zeff*) that reflects the wall's real bending resistance. Analysis reveals that convex curvature amplifies bending capacity by extending the lever arm, mobilizing compressive thrust along the convex face, and redistributing stresses to delay crack localization. The exponential trend of *Zeff* with wall projection underscores a fundamental departure from classical plate theory: planar assumptions underestimate stiffness, while curved walls behave in a bending-dominated, shell-like manner, though true membrane action is precluded by masonry's brittle, heterogeneous nature. Using wall projection as a descriptor provides a practical and physically meaningful measure of curvature effects, allowing designers to quantify geometric stiffening and optimize structural performance. These findings highlight that curvature-induced mechanisms: arch formation, stress redistribution, and lever-arm enhancement can govern structural response more significantly than modifications to constituent material properties, providing a rational basis for predicting and optimizing the performance of curved masonry walls.

The study's limitations stem from material variability, modelling simplifications, experimental constraints, and scope. Locally produced bricks and mortars exhibited natural heterogeneity, limiting generalisability. The adopted Finite Element approach employed uniform material parameters, which may not fully capture bond deterioration, 3D cracking, or moisture effects. Additionally, the study focused solely on convex walls under monotonic out-of-plane loading, precluding direct application to concave geometries, dynamic events, or reinforced systems; all these establish a solid foundation for future, more comprehensive investigations and design applications.

4.1. Future work and recommendations

Future research should focus on improving joint friction and load transfer mechanisms, which could further enhance out-of-plane behaviour, particularly in geometrically complex walls. Quantifying the relative contributions of material strength versus geometric arching would clarify their respective roles in structural capacity, guiding more efficient, resource-conscious design. Full-scale experimental validation remains essential to refine numerical models, verify predictions, and develop reliable guidelines for engineers and practitioners.

5. DECLARATIONS

a) Author contributions

John Mary Joseph Yiga: Conceptualization, Methodology, Software, Validation, Formal analysis, Resources, Data curation, Writing-original draft preparation, Writing-review and editing. Allan Ray Okodi: Conceptualization, Methodology, Validation, Formal analysis, Investigation, Data curation, Writing-original draft preparation, Writing-review and editing, Supervision. Moses Jr. Matovu: Methodology, Validation, Investigation, Writing-original draft preparation, Writing-review and editing, Supervision

b) Funding

The authors declare that this research did not receive funding

c) Data availability

Data will be made available on request.

d) Consent to participate

Not applicable

e) Consent for publication

Not applicable

f) Human and animal rights

This article does not contain any studies with human participants or animals performed by any of the authors

g) Competing interests

The authors declare no competing interests

h) Dual publication

No, results/data/figures in submission have been previously published, or are under consideration for publication elsewhere

i) Clinical trial number

Not applicable.

j) Ethical approval

Not applicable.

REFERENCES

Abdulla, K. F., Cunningham, L. S., & Gillie, M. (2017). Simulating masonry wall behaviour using a simplified micro-model approach. *Engineering Structures*, *151*, 349–365. https://doi.org/10.1016/j.engstruct.2017.08.021

Alejano, L. R., & Bobet, A. (2012). Drucker-Prager criterion. *Rock Mechanics and Rock Engineering*, *45*(6), 995–999. https://doi.org/10.1007/s00603-012-0278-2

Arya, C. (2022). *Design of Structural Elements* (3rd ed). CRC Press. https://doi.org/10.1201/9781003208037

Asteris, P. G., Chronopoulos, M. P., Chrysostomou, C. Z., Varum, H., Plevris, V., Kyriakides, N., & Silva, V. (2014). Seismic vulnerability assessment of historical masonry structural systems. *Engineering Structures*, *62–63*(March), 118–134. https://doi.org/10.1016/j.engstruct.2014.01.031

Avasthi, R., & Rai, D. C. (2021). Behaviour of masonry arch system under various types of loads: state of the art and micro modelling. *14th Canadian Masonry Symposium Montreal, Canada May 16th – May 20th, 2021*, (May). https://www.canadamasonrydesigncentre.com/wp-content/uploads/14th_symposium/115-Avasthi.pdf

Benzeggagh M, K. M. (1996). Measurement of mixed-mode delamination fracture toughness of unidirectional glass/epoxy composites with mixed mode bending apparatus. *Composites Science and Technology , 24*(issue 4 (1996)), 439–448.

Bolhassani, M., Hamid, A. A., Lau, A. C. W., & Moon, F. (2015). Simplified micro modeling of partially grouted masonry assemblages. *Construction and Building Materials*, *83*(March), 159–173. https://doi.org/10.1016/j.conbuildmat.2015.03.021

Briseghella, B., Colasanti, V., Fenu, L., Nuti, C., Spacone, E., & Varum, H. (2019). Seismic Analysis by Macroelements of Fujian Hakka Tulous, Chinese Circular Earth Constructions Listed in the UNESCO World Heritage List. *International Journal of Architectural Heritage*, *14*(10), 1551–1566. https://doi.org/10.1080/15583058.2019.1618973

Campilho, R. D. S. G., de Moura, M. F. S. F., & Domingues, J. J. M. S. (2008). Using a cohesive damage model to predict the tensile behaviour of CFRP single-strap repairs. *International Journal of Solids and Structures*, *45*(5), 1497–1512. https://doi.org/10.1016/j.ijsolstr.2007.10.003

Cavaleri, L., Fossetti, M., & Papia, M. (2009). Modeling of Out-of-Plane Behavior of Masonry Walls. *Journal of Structural Engineering*, *135*(12), 1522–1532. https://doi.org/10.1061/(asce)0733-9445(2009)135:12(1522)

Chang, L. Z., Rots, J. G., & Esposito, R. (2021). Influence of aspect ratio and pre-compression on force capacity of unreinforced masonry walls in out-of-plane two-way bending. *Engineering Structures*, *249*(October), 113350. https://doi.org/10.1016/j.engstruct.2021.113350

D. C. Drucker, W. P. (1952). Soil Mechanics and Plastic Analysis or Limit Design. *Quarterly of Applied Mathematics*, *Volume 10*(Issue 2 (1952)), 157–165. https://doi.org/https://doi.org/10.1090/qam/48291

Debnath, P., Chandra, S., & Mandal, P. (2023). Lateral behaviour of masonry walls with different types of brick bonds , aspect ratio and strengthening measures by polypropylene bands and wire mesh. *Structures*, *49*(September 2022), 623–639. https://doi.org/10.1016/j.istruc.2023.01.155

Elmorsy, M. M., Ghaleb, A. A., & El-Zoughiby, M. E. (2019). Performance-Based Seismic Assessment of Buildings With Curved Shear Walls. *Journal of Engineering Research*, *164*(December), 1–14. https://doi.org/10.21608/ERJ.2019.131347

Fam, A., Shaat, A., Macdougall, C., & Chidiac, S. E. (2015). *Out-of-Plane Bending of Masonry Walls With Near-Surface Mounted and Externally Bonded Reinforcement Out-of-plane bending of masonry walls with near-surface mounted and externally bonded reinforcement *. 7982*. https://doi.org/10.1080/13287982.2010.11465062

Freiherrova, N., & Krejsa, M. (2019). Membrane Structures and Their Use in Civil Engineering. *Transactions of the VŠB – Technical University of Ostrava, Civil Engineering Series*, *18*(2), 1–10. https://doi.org/10.31490/tces-2018-0008

Furtado, A., Rodrigues, H., Arêde, A., & Varum, H. (2020). Effect of the Panel Width Support and Columns Axial Load on the Infill Masonry Walls Out-Of- Plane Behavior E ff ect of the Panel Width Support and Columns Axial Load on. *Journal of Earthquake Engineering*, *24*(4), 653–681. https://doi.org/10.1080/13632469.2018.1453400

Galati, N., Garbin, E., Tumialan, G., & Nanni, A. (2005). Design guidelines for masonry structures: Out of plane loads. *American Concrete Institute, ACI Special Publication*, *SP-230*, 269–288. https://doi.org/10.14359/14837

Gentry, T. R., Cavieres, A., & Al-Haddad, T. (2009). Parametric design, detailing and structural analysis of doubly-curved load-bearing block walls. *11th Canadian Masonry Symposium*. https://www.canadamasonrydesigncentre.com/wp-content/uploads/11th_symposium/C8-2.pdf

Giordano, N., Crespi, P., & Franchi, A. (2017a). Flexural strength-ductility assessment of unreinforced masonry cross-sections: analytical expressions. *Engineering Structures*, *148*, 399–409. https://doi.org/10.1016/j.engstruct.2017.06.047

Giordano, N., Crespi, P., & Franchi, A. (2017b). Flexural strength-ductility assessment of unreinforced masonry cross-sections: analytical expressions. *Engineering Structures*, *148*, 399–409. https://doi.org/10.1016/j.engstruct.2017.06.047

Godio, M., & Beyer, K. (2019). Evaluation of force-based and displacement-based out-of-plane seismic assessment methods for unreinforced masonry walls through refined model simulations. *Earthquake Engineering and Structural Dynamics*, *48*(4), 454–475. https://doi.org/10.1002/eqe.3144

González del Solar, G., Domizio, M., Martín, P., & Maldonado, N. (2023). Modeling of Structural Masonry. In *Masonry for Sustainable Construction* (Vol. 34, p. 23). IntechOpen. https://doi.org/10.5772/intechopen.108155

Gumaste, K. S., Rao, K. S. N., Reddy, B. V. V., & Jagadish, K. S. (2007). Strength and elasticity of brick masonry prisms and wallettes under compression. *Materials and Structures/Materiaux et Constructions*, *40*(2), 241–253. https://doi.org/10.1617/s11527-006-9141-9

Hejazi, M., & Kaviani Dezaki, T. (2023). Influence of imperfection on the failure analysis of masonry arches. In *European Physical Journal Plus* (Vol. 138, Number 1). https://doi.org/10.1140/epjp/s13360-022-03627-1

Hernoune, H., Ouldkhaoua, Y., Benabed, B., Abousnina, R., Vimonsatit, V., Mohammed, A., & Manalo, A. (2025). Micro-Modeling of Polymer–Masonry Wall Composites Under In-Plane Loading. *Journal of Composites Science*, *9*(4). https://doi.org/10.3390/jcs9040179

Heyman, J. (1982). The Masonry Arch. In *Structural Analysis*. John Wiley & Sons Ltd. https://doi.org/10.1017/cbo9780511529580.006

Huang, D., Pons, O., & Albareda, A. (2020). Bond strength tests under pure shear and tension between masonry and sprayed mortar. *Materials*, *13*(9). https://doi.org/10.3390/ma13092183

Huerta, S. (2006). Galileo was wrong: The geometrical design of masonry arches. *Nexus Network Journal*, *8*(2), 25–52. https://doi.org/10.1007/s00004-006-0016-8

Jinwuth, W., Samali, B., & Wang, C. (2011). Pushover testing of circular adobe structure. *Advanced Materials Research*, *287–290*(August 2021), 1907–1910. https://doi.org/10.4028/www.scientific.net/AMR.287-290.1907

Junaid Iqbal, M. (2021). Constitutive Material Model for Block Masonry and Its Mechanical Properties. *Journal of Mechanics of Continua and Mathematical Sciences*, *16*(4). https://doi.org/10.26782/jmcms.2021.04.00005

Kaushik, H. B., Rai, D. C., & Jain, S. K. (2007a). Stress-Strain Characteristics of Clay Brick Masonry under Uniaxial Compression. *Journal of Materials in Civil Engineering*, *19*(9), 728–739. https://doi.org/10.1061/(asce)0899-1561(2007)19:9(728)

Kaushik, H. B., Rai, D. C., & Jain, S. K. (2007b). Uniaxial compressive stress-strain model for clay brick masonry. *Current Science*, *92*(4), 497–501.

Li, Y., & Zeng, B. (2023). Modeling of masonry structures using a new 3D cohesive interface material model considering dilatancy softening. *Engineering Structures*, *277*(December 2022), 115466. https://doi.org/10.1016/j.engstruct.2022.115466

Maccarini, H., Vasconcelos, G., Rodrigues, H., Ortega, J., & Lourenço, P. B. (2018). Out-of-plane behavior of stone masonry walls : Experimental and numerical analysis. *Construction and Building Materials*, *179*, 430–452. https://doi.org/10.1016/j.conbuildmat.2018.05.216

Maria, A., Altri, D., Miranda, S. De, Castellazzi, G., & Sarhosis, V. (2018). A 3D detailed micro-model for the in-plane and out-of-plane numerical analysis of masonry panels. *Computers and Structures*. https://doi.org/10.1016/j.compstruc.2018.06.007

Milani, G., Lourenço, P. B., & Tralli, A. (2006). Homogenised limit analysis of masonry walls, Part I: Failure surfaces. *Computers & Structures*, *84*(3–4), 166–180. https://doi.org/10.1016/j.compstruc.2005.09.005

Misir, I. S., & Yucel, G. (2023). Numerical Model Calibration and a Parametric Study Based on the Out-Of-Plane Drift Capacity of Stone Masonry Walls. *Buildings*, *13*(2). https://doi.org/10.3390/buildings13020437

Nazimi, K., Castro, J. J., Omi, S., & Ali, B. S. (2024). Proposal of Empirical Equations for Masonry Compressive Strength: Considering the Compressive Strength Difference between Bricks and Mortar. *Buildings*, *14*(4). https://doi.org/10.3390/buildings14041138

Noor-E-Khuda, S., Dhanasekar, M., & Thambiratnam, D. P. (2016). An explicit finite element modelling method for masonry walls under out-of-plane loading. *Engineering Structures*, *113*, 103–120. https://doi.org/10.1016/j.engstruct.2016.01.026

Osorio, F. A., Baena, J. F., Jaramillo, J. D., & Acevedo, A. B. (2024). Experimental Evaluation of Brick Unreinforced Masonry Wall Out-of-Plane Capacity and Modeling Using the Yield Line Method. *Iranian Journal of Science and Technology - Transactions of Civil Engineering*, (0123456789). https://doi.org/10.1007/s40996-024-01675-4

Pantò, B., Cannizzaro, F., Caliò, I., & Lourenço, P. B. (2017). Numerical and Experimental Validation of a 3D Macro-Model for the In-Plane and Out-Of-Plane Behavior of Unreinforced Masonry Walls. *International Journal of Architectural Heritage*, *11*(7), 946–964. https://doi.org/10.1080/15583058.2017.1325539

Patel, K. P., & Dubey, R. N. (2022). Effect of flanges on the in-plane behavior of the masonry walls. *Engineering Structures*, *273*(August). https://doi.org/10.1016/j.engstruct.2022.115059

Penner, O., & Elwood, K. J. (2016). Out-of-plane dynamic stability of unreinforced masonry walls in one-way bending: Shake table testing. *Earthquake Spectra*, *32*(3), 1675–1697. https://doi.org/10.1193/011415EQS009M

Plevris, V., & Asteris, P. G. (2014). Modeling of masonry failure surface under biaxial compressive stress using Neural Networks. *Construction and Building Materials*, *55*(March), 447–461. https://doi.org/10.1016/j.conbuildmat.2014.01.041

Ram Parajuli, H., & Ghimire, A. (2021). Investigation on Lateral Loading on Masonry Walls. *Nepal Journal of Science and Technology*, *19*(2), 33–40. https://doi.org/10.3126/njst.v20i1.39385

Rondeaux, J. F., Deschuyteneer, A., & Zastavni, D. (2018). Assessing geometrically the structural safety of masonry arches. *Building Knowledge, Constructing Histories*, *2*, 1129–1136. https://doi.org/10.1201/9780429506208-144

Šakić, B., Marinković, M., Butenweg, C., & Klinkel, S. (2023). Influence of slab deflection on the out-of-plane capacity of unreinforced masonry partition walls. *Engineering Structures*, *276*(November 2022). https://doi.org/10.1016/j.engstruct.2022.115342

Samali, B., Jinwuth, W., Heathcote, K., & Wang, C. (2011). Seismic capacity comparison between square and circular plan adobe construction. *Procedia Engineering*, *14*(April 2017), 2103–2108. https://doi.org/10.1016/j.proeng.2011.07.264

Schneemayer, A., Schranz, C., Kolbitsch, A., & Tschegg, E. K. (2014). Fracture-Mechanical Properties of Mortar-to-Brick Interfaces. *Journal of Materials in Civil Engineering*, *26*(9). https://doi.org/10.1061/(asce)mt.1943-5533.0000955

Shadlou, M., Ahmadi, E., & Kashani, M. M. (2020). Micromechanical modelling of mortar joints and brick-mortar interfaces in masonry Structures: A review of recent developments. *Structures*, *23*(January), 831–844. https://doi.org/10.1016/j.istruc.2019.12.017

Tariq, H., Najafgholipour, M. A., Sarhosis, V., & Milani, G. (2023). In-plane strength of masonry wall panels: A comparison between design codes and high-fidelity models. *Structures*, *47*(November 2022), 1869–1899. https://doi.org/10.1016/j.istruc.2022.11.125

Teschemacher, T., Kalkbrenner, P., Pela, L., & Wu, R. (2023). *An orthotropic damage model for masonry walls with consistent damage evolution laws*. *0123456789*. https://doi.org/10.1617/s11527-023-02220-x

Toshniwal, S., Sluijs, J., Meijers, S. J. H., Sharma, S., & Messali, F. (2024). Engineering methodology to assess the seismic out-of-plane response of two-way spanning unreinforced masonry walls with multiple openings. *Journal of Physics: Conference Series*, *2647*(14). https://doi.org/10.1088/1742-6596/2647/14/142003

Vaculik, J., & Griffith, M. (2017). Out-of-plane load–displacement model for two-way spanning masonry walls. *Engineering Structures*, *141*(October 2019), 328–343. https://doi.org/10.1016/j.engstruct.2017.03.024

Vermeltfoort, A. T., Martens, D. R. W., & Van Zijl, G. P. A. G. (2007). Brick-mortar interface effects on masonry under compression. *Canadian Journal of Civil Engineering*, *34*(11), 1475–1485. https://doi.org/10.1139/L07-067

Wang, C., Sarhosis, V., & Nikitas, N. (2018). Strengthening/Retrofitting Techniques on Unreinforced Masonry Structure/Element Subjected to Seismic Loads: A Literature Review. *The Open Construction and Building Technology Journal*, *12*(1), 251–268. https://doi.org/10.2174/1874836801812010251

Wilding, B. V., & Beyer, K. (2016). Effective stiffness of unreinforced brick masonry walls. *Brick and Block Masonry: Trends, Innovations and Challenges - Proceedings of the 16th International Brick and Block Masonry Conference, IBMAC 2016*, (September), 1993–2002. https://doi.org/10.1201/b21889-248

Xie, X., Qu, Z., Fu, H., & Zhang, L. (2021). Effect of prior in-plane damage on the out-of-plane behavior of masonry infill walls. *Engineering Structures*, *226*(March). https://doi.org/10.1016/j.engstruct.2020.111380

Yiga, J., Matovu, M., & Okodi, A. R. (2025). FEM Analysis of the Effect of Geometrical Radius on the Force Capacity of Unreinforced Masonry walls under Out-Of-Plane Monotonic Loading. *ASRIC Journal on Engineering Sciences*, *6*(1), 37–51.